A Chip-Based "Bipolar" DNA Switch Modulated by Intermolecular Interactions

by

Yiting Tang

M.Sc., Tongji University, 2009
B.Sc., Tongji University, 2006

Thesis Submitted in Partial Fulfillment
of the Requirements for the Degree of
Master of Science

in the
Department of Chemistry
Faculty of Science

SIMON FRASER UNIVERSITY

Spring 2013

Approval

Name: **Yiting Tang**

Degree: **Master of Science (Chemistry)**

Title of Thesis: ***A Chip-Based "Bipolar" DNA Switch Modulated by Intermolecular Interactions***

Examining Committee:

Chair: Dr. Krzysztof Starosta, Associate Professor

Dr. Hua-Zhong (Hogan) Yu
Senior Supervisor
Professor, Department of Chemistry, SFU

Dr. Michael H. Eikerling
Supervisor
Associate Professor, Department of Chemistry, SFU

Dr. Timothy V. Beischlag
Supervisor
Associate Professor, Faculty of Health Sciences, SFU

Dr. Dan Bizzotto
Internal Examiner
Associate Professor, Department of Chemistry, UBC

Date Defended/Approved: March 15, 2013

Partial Copyright Licence

Abstract

Herein, we report a unique “bipolar” DNA switch that integrates an anti-adenosine aptamer (a 12-base mismatch loop) in the middle of a complementary DNA double helix. The electrochemical signal change of methylene blue attached to the distal end of the DNA switch upon ligand binding is dependent on the DNA surface density. At high surface density, it switches on by increasing the peak current; at low surface density, it switches on by decreasing the peak current. No significant change of either the integrated charge (peak area) or the electron transfer rate is observed; only the shape of the reduction peak changes. Rather than by removal of perturbations or by change of surface accessibility, the switching is caused by a change of intermolecular interactions. The high specificity, reusability and stability of the DNA switch suggest the possibility of designing a new class of biosensors in which analyte binding produces large changes in intermolecular interactions.

Keywords: bipolar; DNA; switch; aptamer; electrochemistry; intermolecular interactions

To my family and friends

Acknowledgements

Firstly, I would like to give my sincere gratefulness to my senior supervisor, Dr. Hua-Zhong (Hogan) Yu, for the research opportunities that he has given me and for his guidance, patience and support throughout the years. I have improved myself a lot by learning not only chemistry knowledge but also the way of doing research from him which are invaluable to me.

I would also like to thank Dr. Michael H. Eikerling and Dr. Timothy V. Beischlag for being my committee members – their advice and suggestions have been tremendously helpful to my studies. I also give thanks to Dr. Krzysztof Starosta and Dr. Dan Bizzotto for taking time to be the chair and internal examiner at my defence.

I would also like to thank Dr. Dipankar Sen for the valuable and constructive discussions on my research and papers. I would like to thank Dr. Eberhard Kiehlmann for helping me revise my thesis. My special thanks go to Dr. Bixia Ge for training me and giving me helpful advices for both my research and career. I would like to also thank Dr. Janet Huang for discussions on the project. I am very thankful to the past and present members of the Yu laboratory for their friendship and support.

Finally, I would like to express my deepest thankfulness to my family for their unconditional support and encouragement to me.

Table of Contents

List of Figures

List of Acronyms

A	adenosine nucleoside
ACV	alternating current voltammetry
AMP	adenosine monophosphate
AQ	anthraquinone
ATP	adenosine triphosphate
C	cytidine nucleoside
CC	chronocoulometry
CV	cyclic voltammetry
DM	daunomycin
DNA	deoxyribose nucleic acid
cDNA	complementary DNA
dsDNA	double-stranded DNA
ssDNA	single-stranded DNA
DPV	differential pulse voltammetry
EIS	electrochemical impedance spectroscopy
eT	electron transfer
Fc	ferrocene
G	guanosine nucleoside
GCE	glassy carbon electrode
GMP	guanosine monophosphate
GNP	gold nanoparticle
GNS	graphene nanosheet
HPLC	high pressure liquid chromatography
LB	leucomethylene blue
MECAS	microfluidic electrochemical aptamer-based sensor
MB	methylene blue
MCH	1-mercapto-6-hexanol
NHS	N-hydroxysuccinimide
NMR	nuclear magnetic resonance

PCR	polymerase chain reaction
SAM	self-assembled monolayer
SELEX	systematic evolution of ligands by exponential enrichment
SWNT	single-walled carbon nanotube
SWV	square wave voltammetry
T	thymidine nucleoside
TCEP	tris(2-carboxyethyl)phosphine
TREAS	target-responsive electrochemical aptamer switch
Tris	Tris(hydroxylmethyl)aminomethane
UMP	uridine monophosphate
UV	ultraviolet

1. Introduction

This chapter is a general introduction to functional DNA and the electrochemistry of DNA monolayers; it also summarizes the designs and underlying mechanisms of DNA-based electrochemical switches. The functional DNA incorporated into DNA-based electrochemical switches includes aptamers, DNAzymes, G-quadruplexes and i-motifs. There are three kinds of redox reporters attached to the functional DNA to provide electrochemical signals. The structure-switching designs are classified into three categories based on the type of functional DNA. Signal-switching mechanisms are postulated to explain how structural changes relate to signaling. This chapter describes the fundamental concepts and research background as the basis of the work in this thesis.

1.1. DNA-based switches

DNA as the storage molecule of biological information has remarkable structural and functional properties, in particular the highly specific base-pairing interactions (Figure 1-1), which allows for replication and transcription[1,2]. In the last few decades, it has gained increasing recognition as a powerful and versatile building block for the fabrication of self-assembled nanostructures[3-5]. A variety of DNA-based nanodevices have been designed and synthesized chemically. The first DNA nanomechanical device was based on the B-Z transition (right-handed helix to left-handed helix) of DNA[6] (Figure 1-2). The relative positions of two double-crossover structures connected by a poly-CG sequence were changed by adding $[Co(NH_3)_6]^{3+}$. While DNA nanotechnology has been developed to allow the fabrication of two- and three-dimensional static nanostructures, it still remains challenging to design dynamic nanostructures[7].

DNA-based switches are dynamic DNA structures which can reversibly undergo conformational changes in the absence and presence of certain external stimuli.

Numerous DNA nanodevices have been shown to respond to a variety of stimuli, including pH, small molecules (e.g. salts and metal ions), and macromolecules (e.g. oligonucleotides and proteins)[8-11]. They are often realized by the incorporation of functional DNA such as aptamers, DNAzymes, G-quadruplexes and i-motifs. The following section describes the properties of such functional DNAs that play an essential role in DNA-based switches. They are specific sequences of DNA which adopt tertiary structures capable of various activities including ligand recognition[12-14] and catalysis of chemical reactions[15,16].

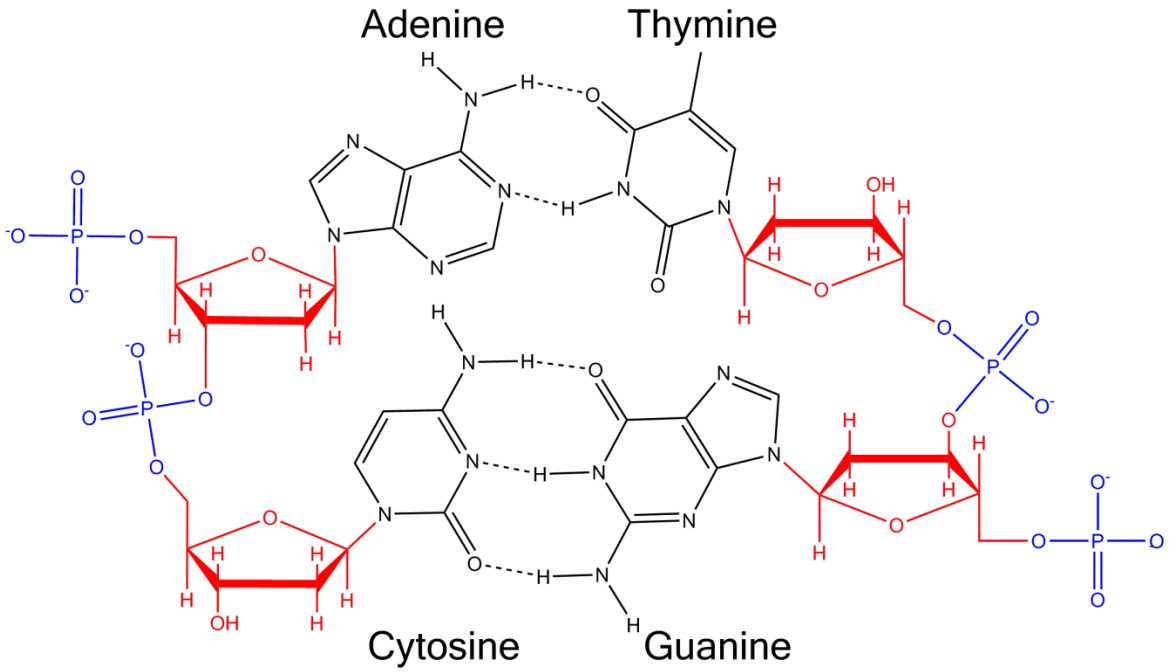

Figure 1-1. Base-pairing interactions of DNA. The ribose, phosphate and aromatic bases are shown in red, blue and black, respectively. Hydrogen bonding between the Watson-Crick base pairs is shown by the dashed lines.

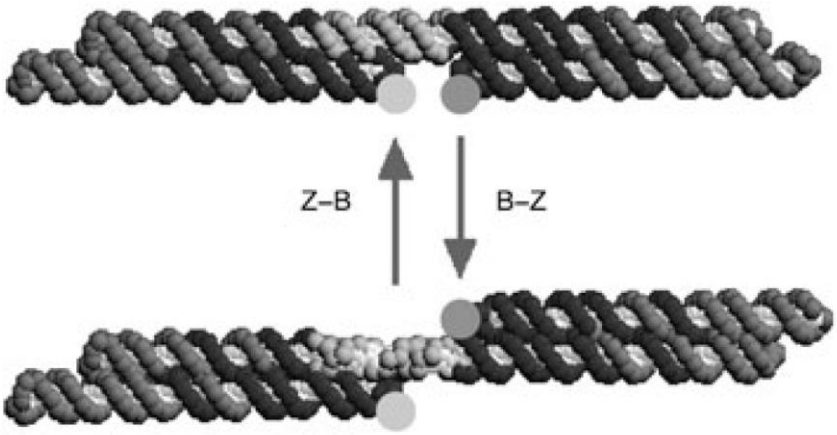

Figure 1-2. Nanomechanical device based on a B-Z transition of DNA. One strand (dark and light gray) forms two double-crossover (DX) arms with two other strands (gray). The hinge (light gray) connecting the arms is a $d(CG)_{10}$ sequence which undergoes a B-Z transition upon addition of cobalt hexammine. Adapted by permission from Macmillan Publishers Ltd: [Nature] (6), copyright (1999).

1.2. Functional DNA

The majority of DNA nanomachines in early years relied on hybridization-induced mechanical motions where the role of DNA was to provide a structural frame and the chosen base sequence determined the movements resulting from configurational changes. Thus, the DNA is relatively passive[17]. To progress to the next stage of complexity, DNA machines should be able to perform functional tasks which require the incorporation of active functional units within these devices. Functional nucleic acids are found in aptamers and DNAzymes. Two other unique DNA structures as active components are G-quadruplexes and i-motifs.

1.2.1. Aptamers

Aptamers are oligonucleotides which bind specifically to target molecules with high affinity. The targets can be organic dyes, amino acids, metal ions, proteins, and even whole cells[18-21]. The affinity range is from micromolar to picomolar. They were first reported independently by Szostak and Gold back in 1990[22,23]. Since then, aptamers have been widely recognized as highly promising tools for a number of important applications[24,25].

DNA aptamers for any given target are obtained by the method of *in vitro* selection called SELEX (systematic evolution of ligands by exponential enrichment)[26-28]. In this method, as shown in Figure 1-3, a random single-stranded DNA library containing different sequences passes through a column where the target molecules are immobilized[27]. Some DNA molecules bind to the target and those that do not bind are washed off. The DNA molecules bound with high specificity are eluted from the column and amplified by PCR (polymerase chain reaction). This process is repeated to produce highly specific target-binding DNA aptamers. Sometimes counter-selection is performed using a secondary target with a similar structure so as to ensure that the successful aptamer is selective only for the desired target. In counter-selection, alternating cycles are carried out and sequences that bind to the secondary target are removed from the selection pool. Once the DNA sequence is obtained, the aptamers can be generated by chemical synthesis. Its binding activity can be confirmed by different methods to validate its affinity and specificity for the target.

Aptamers have many advantages compared to antibodies which are biologically generated proteins[29]. Antibodies require an immune response in host animals to be produced, and aptamers are produced chemically in an oligonucleotide synthesizer in large quantities. Antibodies cannot be obtained for molecules too small to have sufficient binding sites (e.g., metal ions) or for molecules with poor immunogenicity or high toxicity. Although aptamers are selected for target binding *in vitro*, they may be also capable of binding to their targets *in vivo* with good affinity. Besides, aptamers are readily chemically modified, which allows for ease of immobilization onto substrates. For example, in electrochemical detection the electrode substrate is commonly gold. Modification with a thiol group enables the formation of robust DNA monolayers on a gold electrode via sulfur-gold linkages. As a result, the properties of DNA immobilized on gold electrodes are very well characterized[30-32].

The secondary structures of aptamers tend to be very important to the binding affinity and specificity. DNA aptamers often undergo a conformational change upon binding[33,34]. They can fold to internal loops, three-way junctions or G-quartet structures according to their sequences and the structures of the target molecules they are binding. This capability of folding upon binding ensures the high affinity of aptamers for their targets. Small target molecules can incorporate into the nucleic acid folding structure.

For larger target molecules such as some very large proteins, the folding structure of DNA aptamers may integrate into the targets. This is also why DNA aptamers are commonly comprised of single-stranded DNA[35]. However, given the sequences of the selected aptamers, two-stranded DNA aptamers can also be designed to bind to target molecules with similar affinity[36].

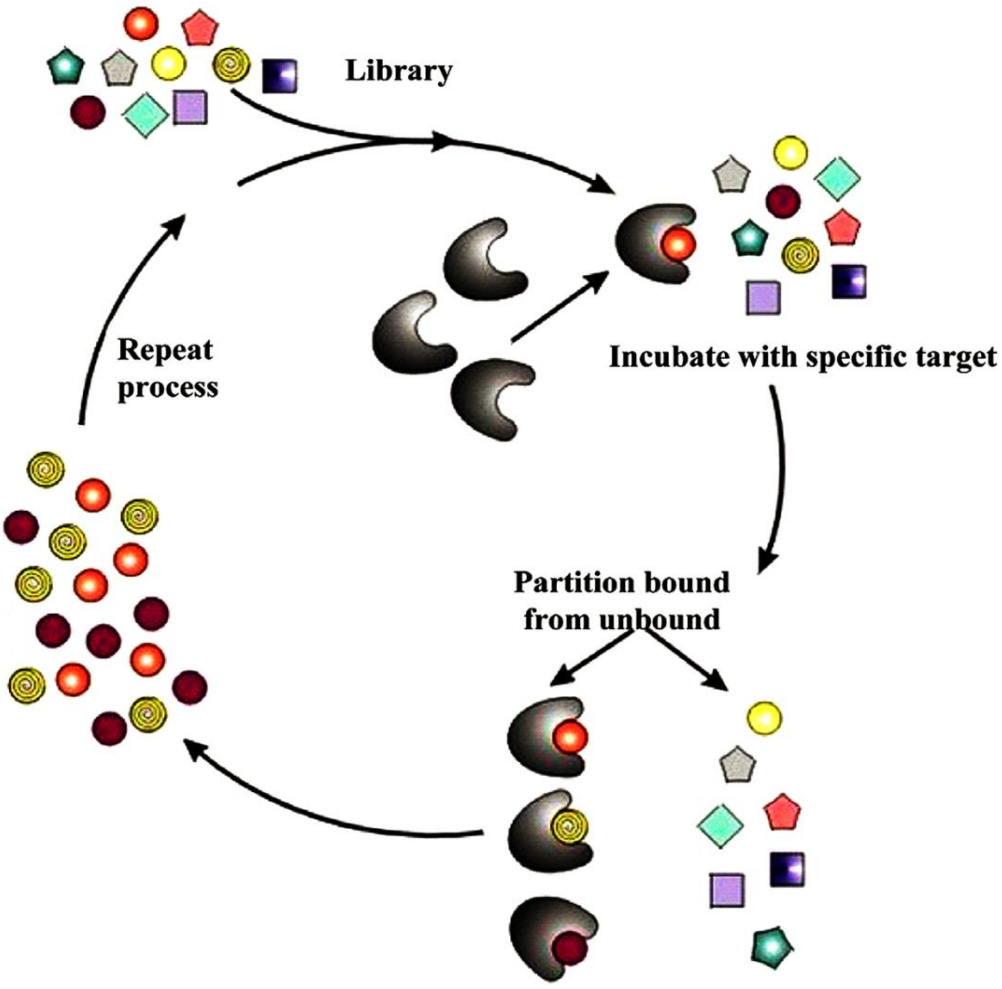

Figure 1-3. The systematic evolution of ligands by exponential enrichment (SELEX) process to isolate nucleic acid aptamers from a large random sequence pool. Reprinted from Trends Anal. Chem. 25, Hamula, et al. "Selection and analytical applications of aptamers", 681-691, copyright (2006), with permission from Elsevier.

The functionality of aptamers has been used in the construction of DNA nanomachines that can controllably bind and release a target molecule. In principle,

such a nanodevice can be constructed to bind any protein or ligand for which an aptamer exists. They are also widely regarded as ideal recognition elements for biosensor applications including environmental monitoring, food analysis, and medical diagnostics[37,38].

1.2.2. DNAzymes

DNAzymes are DNA molecules that catalyze chemical and biological reactions including cleavage, ligation, peptide bond formation and so on[39]. Although natural DNAzymes can be found, the majority of them have been created by *in vitro* evolutionary selection techniques (SELEX) like aptamers. Since the early 1990s, DNAzymes have been reported to possess catalytic activities toward specific substrates. At present, many different DNAzymes have been screened, such as metal-ion-dependent DNA-cleaving DNAzyme, histidine-dependent DNAzyme and DNA ligase DNAzyme[40-42].

These DNAzymes became new members of the enzyme family, joining protein enzymes and ribozymes. However, because of their unique characteristics, DNAzymes exhibit many intrinsic advantages over conventional protein enzymes, including cost-effective synthesis, high chemical stability, and easy chemical modification[43]. Also, most DNAzymes can be denatured and renatured many times without losing their binding ability or activity toward substrates. All these features have made DNAzymes particularly attractive in diverse areas for versatile applications such as biosensing, nanomachines, and logic gate applications[44].

1.2.3. G-quadruplexes and i-motifs

G-quadruplexes are guanine-rich DNA sequences which involve the enthalpically favorable reorganization of guanines to form planar structures through hydrogen bonding[45]. The quadruplex structure is further stabilized by the presence of a metal cation, especially a potassium ion, which sits in the central channel between pairs of guanine tetrads (Figure 1-4). The G-quartet secondary structure exists in many aptamers. For example, the thrombin-binding aptamer selected by Bock et al[46] has been shown by both NMR and X-ray crystallography that it will fold into a G-quartet structure both in the presence of stabilizing salts and upon target binding (Figure 1-5)[47].

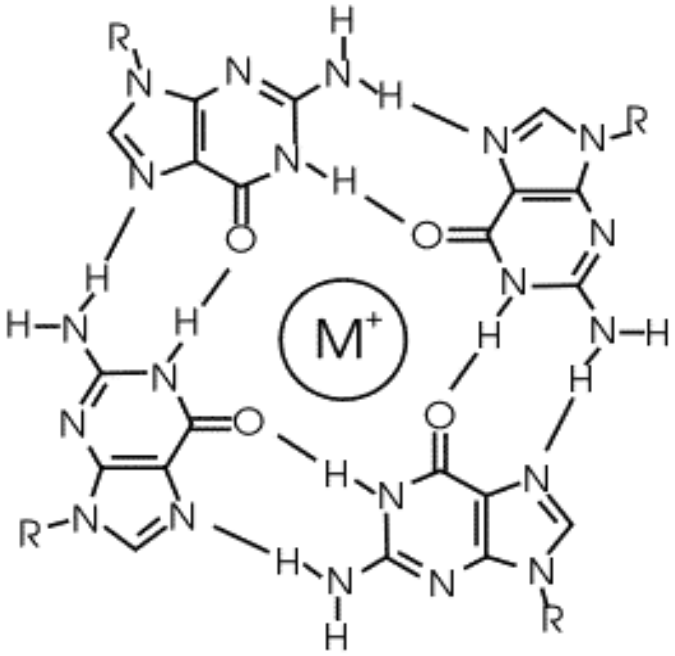

Figure 1-4. The secondary structure of a G-quartet with a metal cation sitting in the central channel.

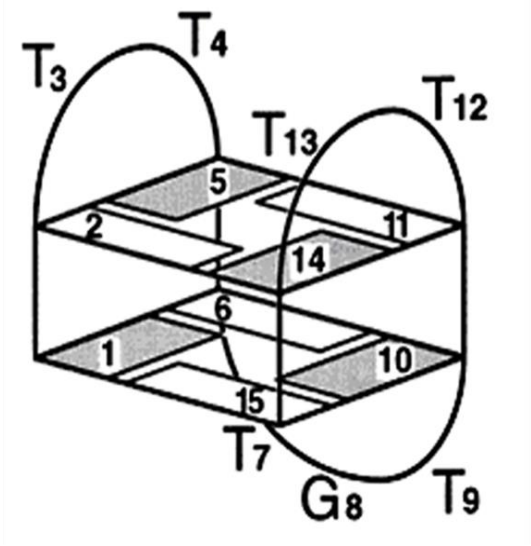

Figure 1-5. Tertiary structure of a thrombin aptamer which forms a G-quadruplex; positions correlate to the sequence. Reprinted from J. Mol. Biol. 256, Kelly, et al. "Reconciliation of the X-ray and NMR structures of the thrombin-binding aptamer d(GGTTGGTGTGGTTGG)", 417-422, copyright (1996), with permission from Elsevier.

In a similar fashion, an i-motif structure was discovered by Guéron and co-workers in 1993[48], in which four DNA strands are held together by an unconventional base pair between a protonated and an unprotonated cytosine base. The difference to a G-quadruplex is that the formation of an i-motif is fuelled by protons rather than by metal ions. It utilizes the fact that cytidine can be protonated at the N3 position at low pH values (pKa = 4.2). These protonated bases can form additional non-Watson-Crick base pairs, for example C-C^+. The incorporation of these conformations into DNA nanomachines, in which an i-motif switches the conformation of the structure in response to pH changes (Figure 1-6), was first demonstrated by Liu and Balasubramanian[49]. Below pH 6.5, the C-rich DNA strand assumes an intramolecular quadruplex conformation in which C-C^+ base pairs occur in a staggered arrangement. At higher pH values, the C-rich DNA strand hybridizes with its complementary strand. Therefore, the DNA conformation can be cycled between an extended duplex state and a closed quadruplex state by subsequent addition of hydrogen or hydroxide ions.

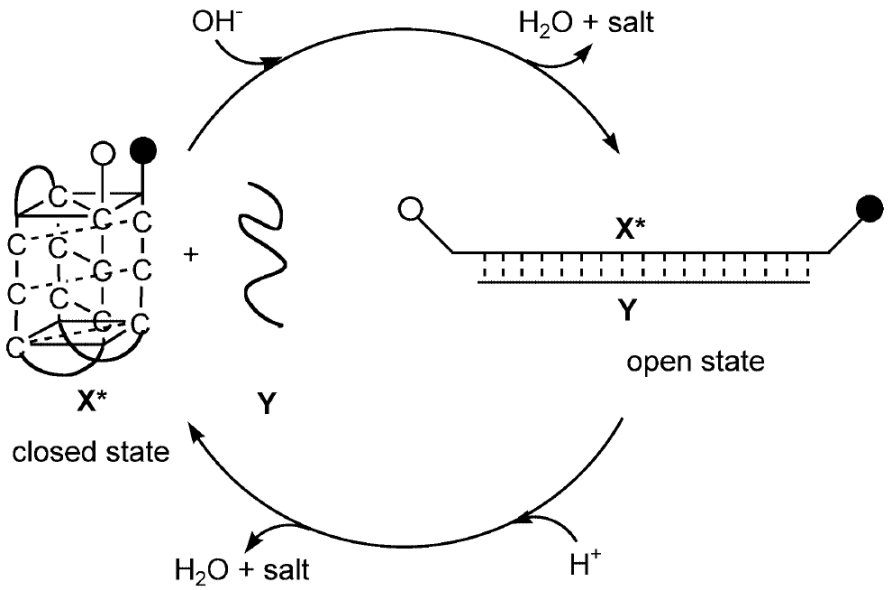

Figure 1-6. A proton-fuelled DNA nanodevice based on the formation of an i-motif. At low pH, the i-motif effectively reduces complementary base pairing between the two single strands. Copyright (2003) WILEY-VCH Verlag GmbH & Co. KGaA, Weinheim. Reproduced with permission from reference [49].

1.3. Electrochemistry of DNA monolayers

For DNA nanodevices, the transduction of the switching event to a measurable signal is important and usually in an optical form or an electrical form. However, because the fluorescence-based readout of DNA nanodevices involves not only highly precise and expensive instrumentation but also sophisticated numerical algorithms to interpret the data, these methods have been generally limited to use in research laboratories. Recently, an impressive number of inventive designs for DNA-based electrochemical switches have appeared[50]. These types of devices combine DNA monolayers with electrochemical transducers to produce a signal and are promising to provide a simple, accurate and inexpensive platform for various applications such as medical diagnosis and environmental detection.

1.3.1. Advantages of electrochemical methods

A typical electrochemical device monitors electrical current variations produced by redox reactions occurring on the electrode surface . Electrochemical methods have

many advantages such as simplicity, rapidity, low cost and high sensitivity; they have been widely used for studying not only small molecules but also large proteins and even cells[51-53]. Because electrochemical reactions give an electronic signal directly, expensive signal transduction equipment is not needed. Moreover, because immobilized species can be readily confined to the surfaces of electrode substrates, miniaturized and portable systems can be developed for clinical testing and on-site environmental monitoring.

For DNA-based electrochemical switches, one of the most often used electrode materials is gold, on which thiolated DNA strands can be immobilized via strong sulfur-gold linkages[30-32] (Figure 1-7). The modification of DNA with a terminal thiol can be easily achieved by simple phosphoramidite chemistry. The DNA immobilization on a gold surface can be readily accomplished by immersing a cleaned gold slide in a DNA solution to form a self-assembled monolayer (SAM). Mixed monolayers formed from alkanethiol alcohols create modified gold electrodes with significantly better electrochemical response than those comprised purely of alkanethiol-DNA[54]. The use of longer alkanethiols to passivate DNA-modified gold electrode surfaces has been found to give electrodes that are more orderly and more stable during long-term dry storage[55], whereas shorter alkanethiol monolayers have better electron transfer properties[55,56]. 1-Mercapto-6-hexanol (MCH) is currently the most common alkanethiol alcohol used to treat DNA-modified surfaces[56] due to its optimal passivation properties.

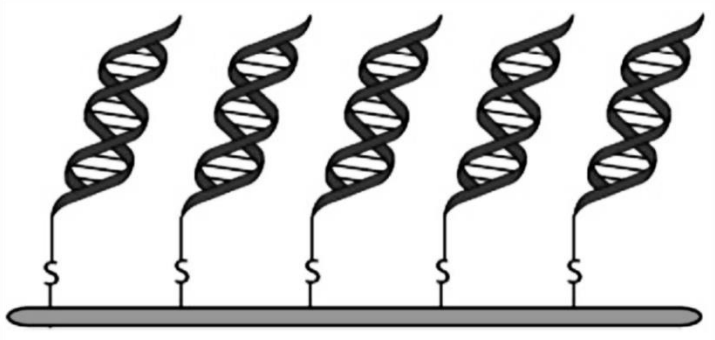

Figure 1-7. Schematic illustration of DNA duplexes in a close-packed monolayer immobilized on gold via alkanethiols. Reprinted with permission from [32]. Copyright (2008) American Chemical Society.

1.3.2. Redox labeling methods on DNA

DNA has been used extensively as material for the fabrication of electrochemical devices because it is easily labeled, chemically stable and readily available. Sensitive electrochemical signaling is usually based on the redox reactions of reporter molecules confined to the electrode surface. Different redox labeling methods on DNA have been developed. A DNA sequence can be directly labeled with a redox reporter molecule through a covalent linker or intercalation. Besides, the solution-diffused redox reporters can also undergo redox reactions on the surface. The change in the electrochemical response of the redox reporter therefore signals the switching event occurring in a DNA nanostructure.

1.3.2.1. Covalently tethered systems

Various reporters, including ferrocene (Fc) and methylene blue (MB), have been covalently tethered to the distal terminus of DNA through flexible alkyl linkages. This has some advantages: because the mobility of the redox reporters is restricted, their position in the DNA monolayer can be controlled by changing the DNA orientation or surface density. Moreover, when the length of linkages is limited, the redox reactions of reporters can only be surface-controlled process without the consideration of diffusion process which simplifies the interpretation of electrochemical data. Third, there is usually only one redox reporter on each single- or double-stranded DNA; therefore, it can be used to quantify the amount of DNA in 1:1 ratio on the electrode surface.

The protocols for the covalent tethering of Fc and MB have been established[57,58]. They involve the preparation of amino-modified DNA oligonucleotide and attachment of the redox reporter via terminal phosphodiester linkers. For Fc, the synthesis and purification of N-hydroxysuccinimide (NHS) ester of ferrocenecarboxylic acid have to be carried out. For MB, the NHS ester of N-(carboxypropyl)methlyene blue is prepared. Since the activated ester is unstable, it must be freshly prepared directly before tethering to the amino-modified DNA. The chemical structures of Fc- and MB-tethered DNA are shown in Figure 1-8.

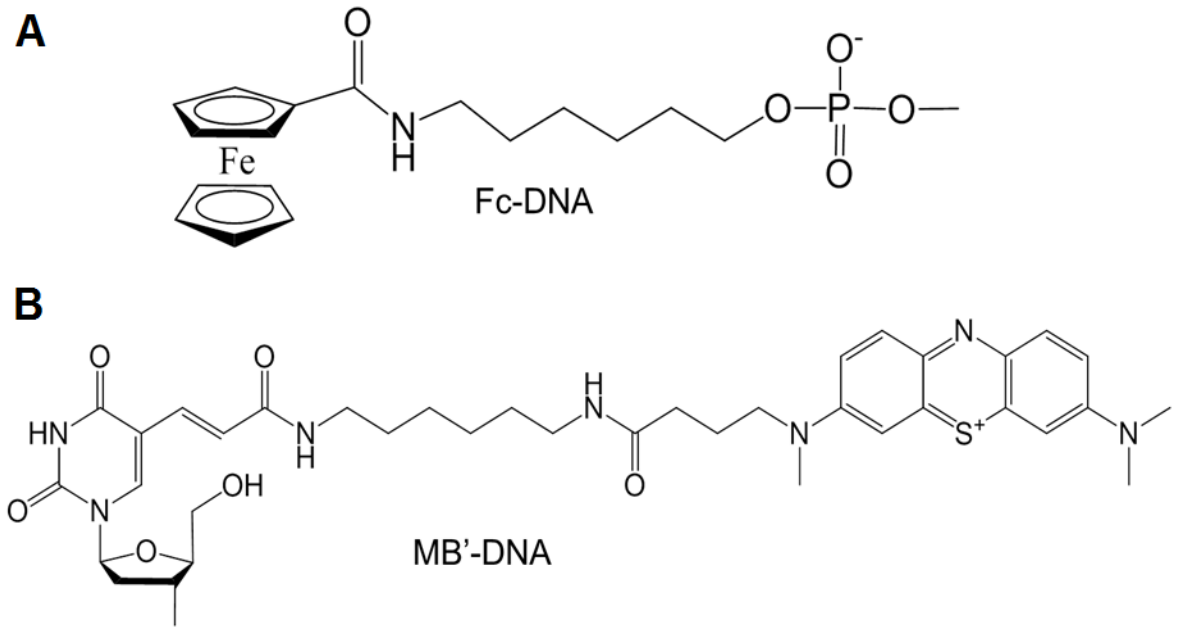

Figure 1-8. Chemical structures of (A) Fc- and (B) MB-tethered DNA. (A) Reprinted from Nucleic Acids Res. 24, Ihara, et al. "Ferrocene-oligonucleotide conjugates for electrochemical probing of DNA", 4273-4280, copyright (1996), with permission from Oxford University Press. (B) Reprinted with permission from [58]. Copyright (2012) American Chemical Society.

1.3.2.2. Intercalation-based systems

Intercalation is the insertion of a ligand between the base pairs of a DNA duplex (Figure 1-9), a non-covalent interaction. The ligands, called intercalators, are mostly polycyclic, aromatic, and planar. Intensively studied DNA intercalators include daunomycin (DM) and methylene blue (MB). In a typical assay, thiolated DNA duplexes with matched or mismatched sequences are first self-assembled on a gold surface, and then treated with micromolar concentrations of a redox-active intercalator. Upon intercalation, the reporter can be electrochemically reduced or oxidized.

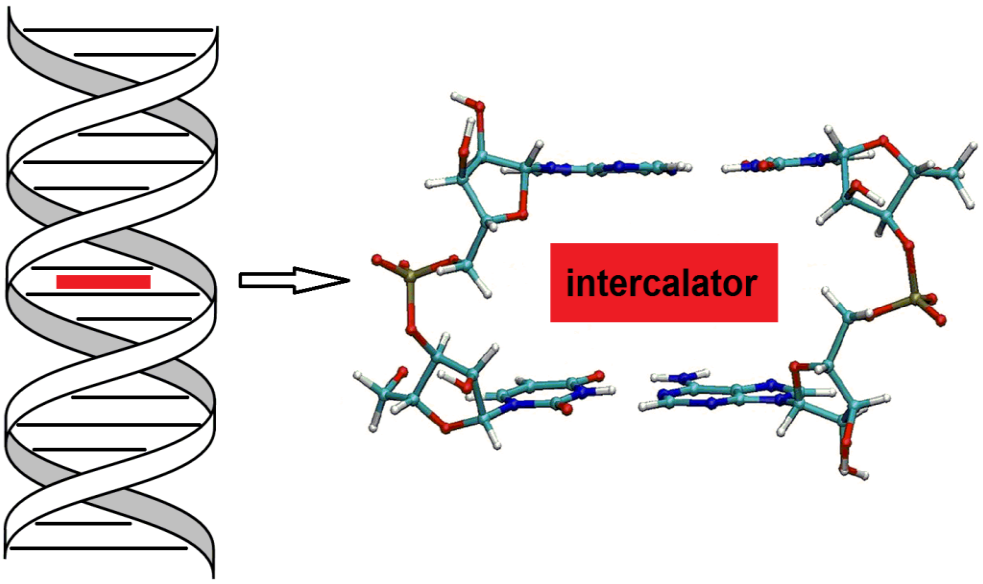

Figure 1-9. Intercalation of a planar molecule in dsDNA. The intercalator molecule and DNA base pairs are represented by the red rectangle and black solid lines, respectively.

Intercalated redox reporters are widely used for the studying DNA-mediated charge transport. The intercalator is not used to report the amount of DNA on the surface or to distinguish between double- and single-stranded DNA. Instead, the coupling of intercalators into the π-stack of DNA critically affects the DNA electrochemistry at long range. It has been demonstrated that the electrochemical signals of redox reporters are sensitive to DNA structure and subtle perturbations in base stacking[59,60]. Structural DNA damages, mismatches and even protein binding result in less efficient current flow.

It has been reported that DNA intercalators like DM or MB bind predominantly near the solvent-exposed terminus of the double-stranded DNA monolayer[61]. The diffusion of intercalators into the monolayer is inhibited by the tight packing of the DNA duplexes at high surface density. Thus intercalators appear to be constrained to the top of closely packed monolayers. However, at lower surface density, a larger signal is obtained for a redox-active DNA intercalator, which is likely due to increased access to the interior of the monolayer.

1.3.2.3. Solution-diffused systems

Negatively charged redox reporters which are freely diffusing in solution can get into close proximity with the electrode surface due to electrostatic interactions. For example, $[Fe(CN)_6]^{3-/4-}$ ions in solution are electrostatically repelled by the negatively charged DNA phosphate backbone and cannot get close to electrode surface leading to a high electron transfer resistance which is detected by the method of electrochemical impedance spectroscopy (EIS)[62]. However, upon incubation or binding to positively charged proteins, the diffusion of $[Fe(CN)_6]^{3-/4-}$ ions toward the electrode surface is facilitated which decreases the electron transfer resistance.

Another solution-based system, $[Ru(NH_3)_6]^{3+}$, is often used as a reliable method to report the amount of DNA on the electrode surface[63,64]. The $[Ru(NH_3)_6]^{3+}$ cations diffuse to the electrode surface and bind electrostatically to the DNA backbone. Their characteristic redox reactions provide the electrochemical readout. DNA dehybridization can be detected by a decreased signal from a higher surface concentration of electrostatically bound $[Ru(NH_3)_6]^{3+}$ as result of the lower negative charge density at the dehybridized surface (Figure 1-10). Besides, the surface densities of both single- and double-stranded oligonucleotides can be accurately determined by integration of the reduction peak of $[Ru(NH_3)_6]^{3+}$ to $[Ru(NH_3)_6]^{2+}$. After incubation in 5.0 μM $[Ru(NH_3)_6]^{3+}$, the surface concentration of $[Ru(NH_3)_6]^{3+}$, Γ_{Ru}, can be calculated using the following equation:

$$\Gamma_{Ru} = \frac{Q}{nFA} \qquad \text{(Equation 1-1)}$$

where Q is the charge obtained by integrating the reduction peak area of surface-bound $[Ru(NH_3)_6]^{3+}$, n is the number of electrons involved in the redox reaction (which is 1), F is Faraday's constant, and A is the electrode area. This equation assumes the following[65]: the interaction between $[Ru(NH_3)_6]^{3+}$ is purely electrostatic, there is complete exchange of $[Ru(NH_3)_6]^{3+}$ with compensation by Na^+ ions; full saturation of DNA-modified surface with $[Ru(NH_3)_6]^{3+}$ occurs at 5.0 μM; the cation exists and binds in the oxidized form [i.e., the cation is (electro)chemically stable]; and every phosphate molecule is accessible for electrostatic binding to the cations.

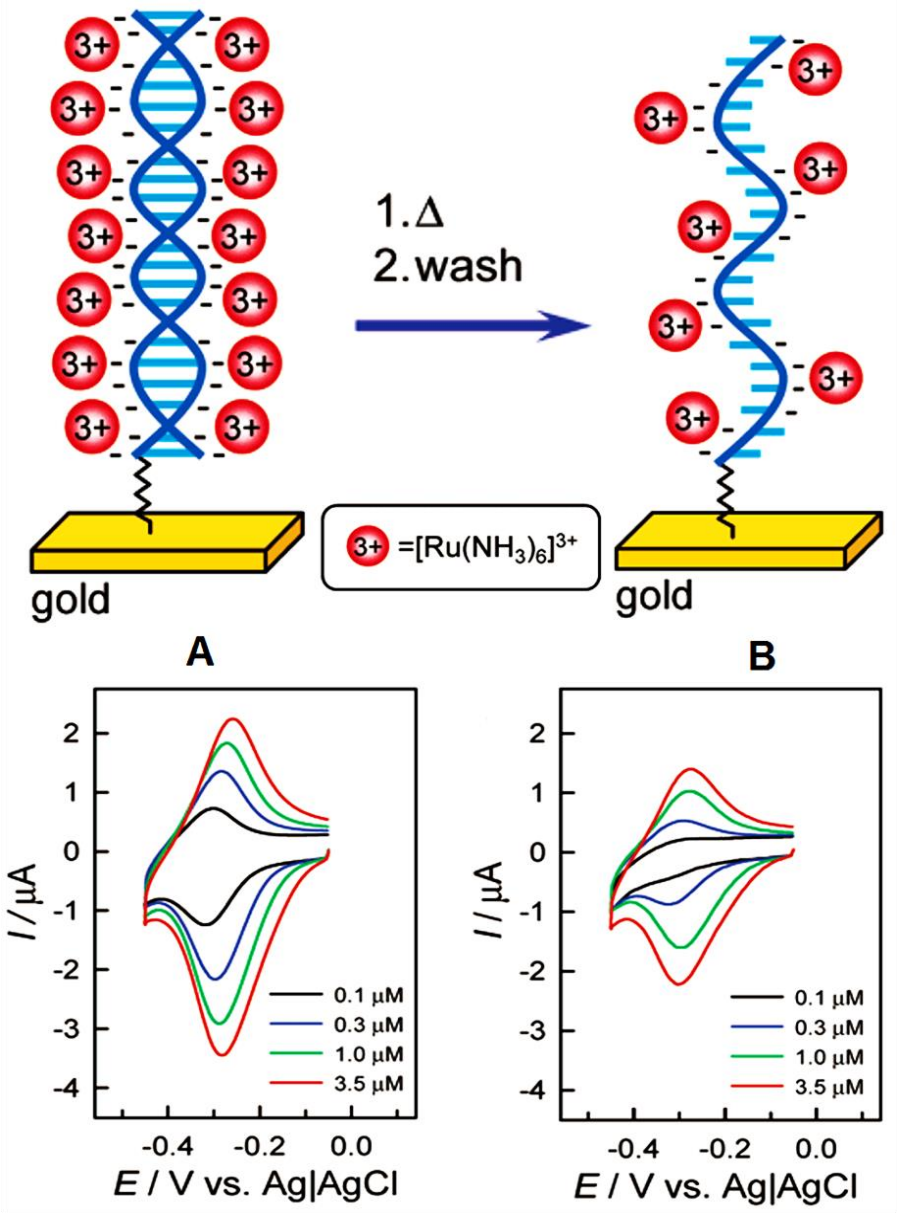

Figure 1-10. Schematic representation and voltammetric response of $[Ru(NH_3)_6]^{3+}$ at different concentrations electrostatically bound (A) to dsDNA- and (B) to ssDNA-modified gold electrodes in 10 mM Tris buffer (pH 7.4). The scan rate = 50 mV/s. Reprinted with permission from [63]. Copyright (2003) American Chemical Society.

Under saturation conditions (i.e., the highest possible concentration of surface-bound $[Ru(NH_3)_6]^{3+}$ was achieved), the measured value can be converted to the surface density of DNA, Γ_{DNA}, using the following equation:

$$\Gamma_{DNA} = \Gamma_{Ru}(\frac{z}{m})N_A \qquad \text{(Equation 1-2)}$$

where *z* is the valence of the redox cation (which is 3), and *m* is the number of nucleotides in the DNA. This equation has the same assumptions and conditions as Equation 1-1.

1.4. Structure-switching designs of DNA-based electrochemical switches

In functional DNA-based electrochemical switches, DNA constructs undergo structural or conformational changes in the presence of external stimuli leading to an electrochemical signal change. In this section, the functional DNA-based electrochemical switches are classified into three categories based on the type of functional DNA. Different types of functional DNA-based electrochemical switches that utilize these designs are described: aptamer-ligand binding, DNAzyme substrate cleavage, and quadruplex formation.

1.4.1. Aptamer-ligand binding

When the DNA constructs immobilized on gold electrode surfaces are incorporated with DNA aptamer sequences, the binding of aptamer to ligand will cause structural switching. With redox-active reporters, the signal change is monitored by electrochemical methods. The DNA constructs are either double-stranded or single-stranded in which the ligand binding induces the dissociation of duplexes or the folding of single strands. Since aptamers have been selected for a variety of ligands, these aptamer-based switches can be used for the quantitative detection of ligands.

1.4.1.1. Dissociation of double-stranded DNA constructs

DNA aptamers selected successfully by *in vitro* selection experiments (SELEX) have a high affinity to their ligands. Thus, single-stranded aptamers may participate in two different kinds of molecular recognition events: (i) binding to their ligand; and (ii) binding to their Watson-Crick complementary strand. This competition can be used to construct DNA aptamer-based switches. This type of switch starts from a fully or partially double-stranded DNA construct with one strand having an aptamer sequence. Upon incubation of ligand, the aptamer strand prefers to bind to the ligand rather than to its complementary strand which leads to the dissociation of the DNA duplex. After each detection, the switch can be regenerated by hybridization with the leaving strand in the absence of ligand.

The adenosine aptamer selected by Huizenga and Szostak in 1995[66] has been used extensively in this type of switch. This aptamer binds adenosine, adenosine monophosphate (AMP) and adenosine triphosphate (ATP) with similar affinities. The binding of two adenosine molecules results in the folding of the aptamer strand and formation of a partially double-stranded region (Figure 1-11)[67]. Researchers have taken advantage of this unique tertiary structure to design and develop aptamer-based biosensors or switches[68]. Zuo et al.[69] modified the surface-bound aptamer strand with ferrocene which hybridized with its fully complementary strand. In its initial state, ferrocene was far from the electrode surface. Upon binding of the aptamer with ATP, the aptamer strand dehybridized from the double helix and folded back, bringing the ferrocene closer to the electrode (Figure 1-12A). A remarkable increase in the current monitored by square wave voltammetry (SWV) was observed on increasing the concentration of ATP. With an aptamer strand modified by ferrocene close to the electrode surface, Liu et al.[70] observed that upon binding to adenosine, the aptamer strand dissociated from the surface-bound partially complementary strand, and the electrochemical signal of ferrocene decreased as characterized by cyclic voltammetry (CV) (Figure 1-12B).

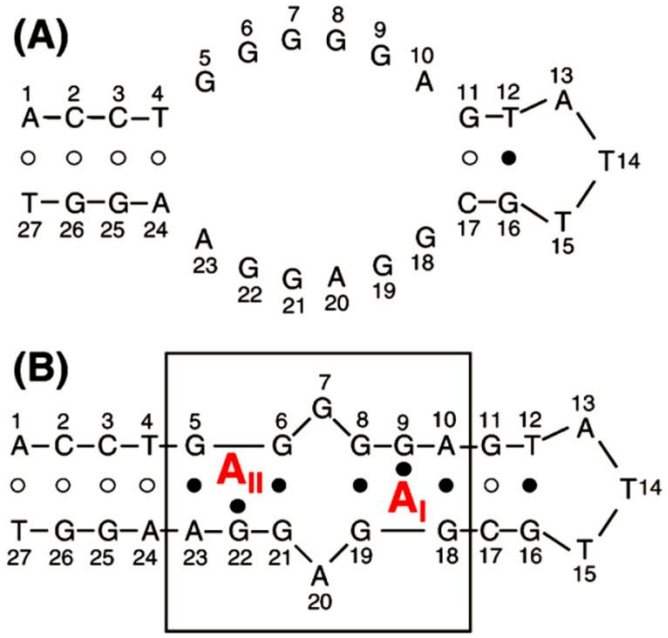

Figure 1-11. Secondary structure of adenosine aptamer (A) before and (B) after binding to adenosine at the two non-equivalent sites (A_I and A_{II}). Reprinted from J. Chem. Biol. 4, Lin, et al. "Structural basis of DNA folding and recognition in an AMP-DNA aptamer complex: distinct architectures but common recognition motifs for DNA and RNA aptamers complexed to AMP", 817-832, copyright (1997), with permission from Elsevier.

Redox labeling methods other than covalent tethering have also been used in aptamer-based switches, including solution-diffused and intercalated redox reporters. The dissociation of a partial double-stranded DNA construct results in the decrease of integrated charge of the surface-bound $[Ru(NH_3)_6]^{3+}$ cations which can be monitored by chronocoulometry (CC)[71,72] and cyclic voltammetry (CV)[72]; and the decrease of electron transfer resistance can be monitored by electrochemical impedance spectroscopy (EIS)[73]. Another adenosine aptamer-based switch is based on a specific interaction of MB with guanine[74]. The dissociation of aptamer strands moves MB molecules into bulk solution causing a current decrease which can be monitored by differential pulse voltammetry (DPV). The partial duplex can be regenerated at least five times by hybridization with aptamer strands.

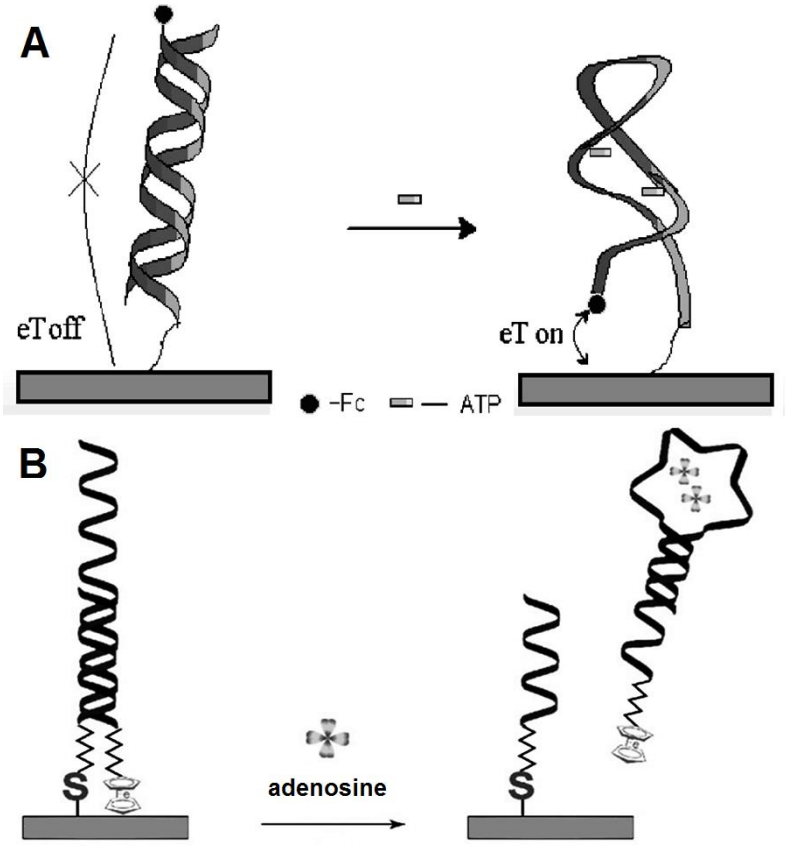

Figure 1-12. Double-stranded aptamer-based electrochemical switches with covalently tethered ferrocene based on duplex dissociation upon adenosine/ATP binding. Ferrocene is modified at the (A) distal and (B) proximal end of the aptamer strand. (A) Reprinted with permission from [69]. Copyright (2007) American Chemical Society. (B) Reprinted from Electrochim. Acta 54, Liu, et al. "Highly sensitive, reusable electrochemical aptasensor for adenosine", 6207-6211, copyright (2009), with permission from Elsevier.

Unlike the adenosine aptamer, the anti-thrombin aptamer is known to fold into a compact G-quadruplex upon thrombin binding[75-77]. Lu et al.[78] immobilized double-stranded DNA constructs in which the aptamer strand was not labeled, while the complementary strand was labeled with ferrocene at the distal end and with thiol at the proximal end. Upon binding thrombin, the aptamer strand dissociated from the surface; the complementary strand then folded into a hairpin in the presence of Mg^{2+}, and the ferrocene moved closer to the electrode surface resulting in a higher electrical current (Figure 1-13). When the anchored strand on the surface was the aptamer strand, the

complementary strand was released, along with its tethered ferrocene. A decrease in the current was observed in the presence of thrombin[79]. These surfaces are also reusable with regeneration by repeating the on-chip hybridization of the leaving DNA strand. The detection limit of thrombin by these designs is as low as 2 nM.

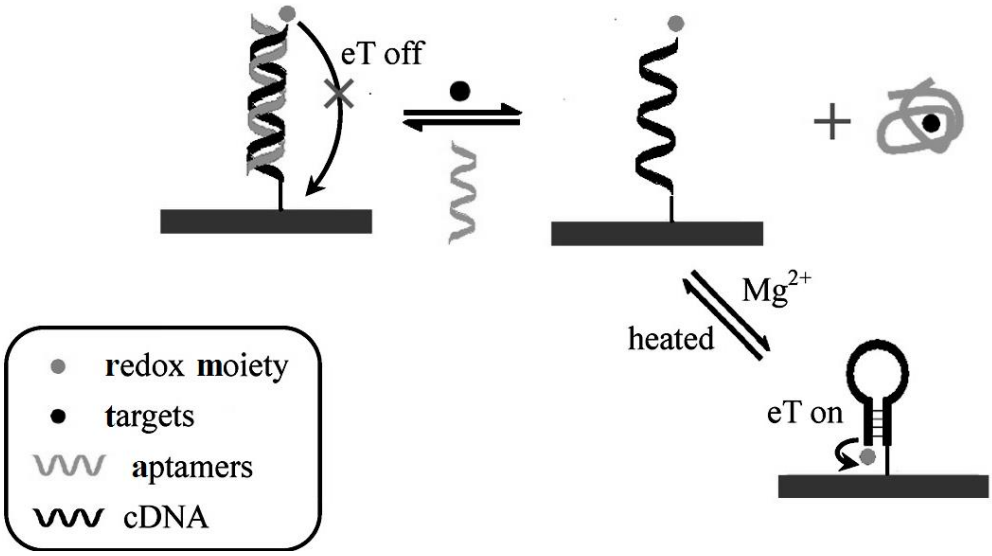

Figure 1-13. Aptamer-based electrochemical switch based on the formation of a hairpin structure with ferrocene attached at the distal end of the complementary strand. Reprinted with permission from [78]. Copyright (2008) American Chemical Society.

1.4.1.2. Folding of single-stranded DNA constructs

For aptamer-based switches consisting of single-stranded DNA, the advantages over double-stranded DNA are (1) the conformational changes of DNA upon ligand binding are simple and do not involve dissociation of the duplex; (2) regeneration of the surface is easier and does not require rehybridization of the dissociated strand.

A single-stranded aptamer strand immobilized on a gold electrode surface folds to a unique tertiary structure in the presence of ligand. Plaxco et al.[80,81] designed two aptamer-based electrochemical switches against the protein thrombin and the small molecule cocaine, respectively (Figure 1-14). Each is comprised of a specific DNA aptamer which is modified at its 5'-terminus with a thiol group and at its 3'-terminus with

a redox-active methylene blue (MB) molecule. In the absence of ligand, the aptamers are thought to be entirely (thrombin) or partially (cocaine) unfolded. However, upon ligand binding, the aptamer folds into a G-quadruplex (thrombin) or three-way junction (cocaine), which changes the position of the redox reporter relative to the electrode surface. When MB moves farther from the gold surface upon thrombin binding, a decrease in the electrochemical current can be measured by alternating current voltammetry (ACV); when MB moves closer to the gold surface upon cocaine binding, the current increases. The regeneration can be easily realized by simple washing using 6M guanidine hydrochloride in the case of thrombin, or immersion in ligand-free buffer for the cocaine detection.

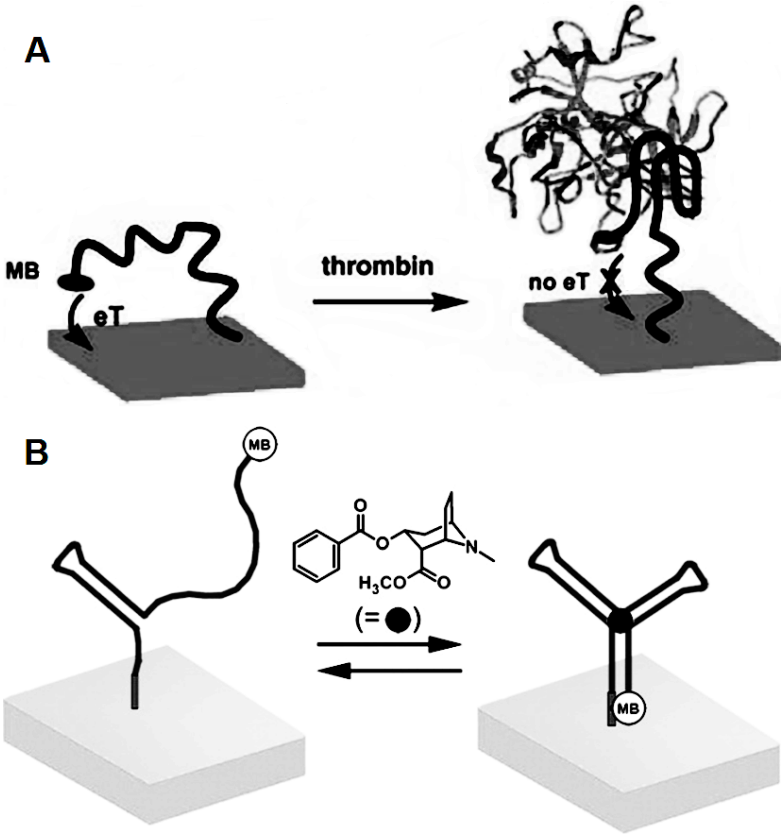

Figure 1-14. Single-stranded aptamer-based electrochemical switches with covalently tethered methylene blue based on folding of the aptamer strand upon ligand binding: (A) thrombin; (B) cocaine. (A) Copyright (2005) WILEY-VCH Verlag GmbH & Co. KGaA, Weinheim. Reproduced with permission from reference [80]. (B) Reprinted with permission from [81]. Copyright (2006) American Chemical Society.

In contrast to the thrombin aptamer-based electrochemical switch of the Plaxco group, Radi et al.[82] designed an electrochemical switch using a shorter 15-nucleotide thrombin aptamer and, as a result, the electrochemical signal does not decrease but rather increase with increasing concentrations of thrombin. The aptamer was immobilized via the 5'-thiol group onto a gold electrode which was then passivated with 2-mercaptoethanol, forming a mixed monolayer. Because of the short length of the aptamer, folding of the aptamer upon thrombin binding brought the 3'-ferrocene moiety closer to the electrode surface, thus increasing the electrochemical signal (Figure 1-15). The switch was then characterized using cyclic voltammetry (CV), differential pulse voltammetry (DPV), and electrochemical impedance spectroscopy (EIS). Also, the switch could be fully regenerated by simply unfolding the aptamer in 1.0 M HCl, and there was no loss in electrochemical signal upon subsequent thrombin binding after being regenerated up to 25 times.

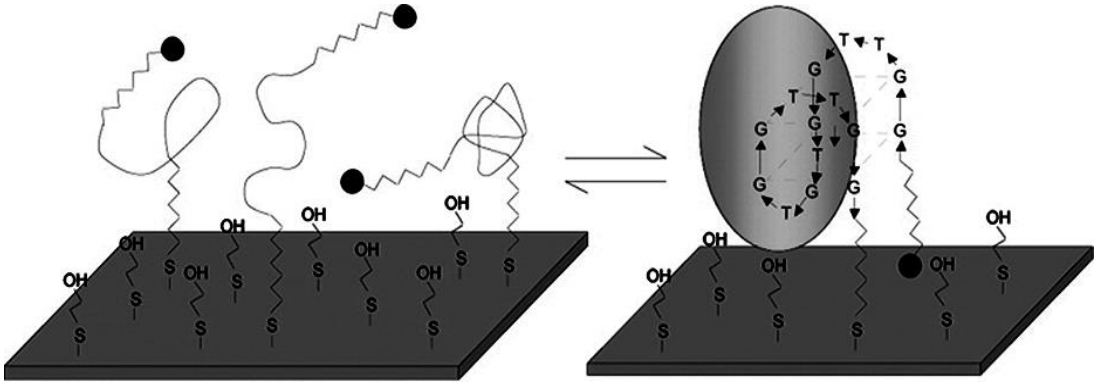

Figure 1-15. A short thrombin aptamer-based electrochemical switch. Thrombin binding folds the aptamer into a G-quartet structure, bringing the ferrocene close to the electrode surface. Reprinted with permission from [82]. Copyright (2006) American Chemical Society.

1.4.2. DNAzyme substrate cleavage

DNAzyme-based electrochemical devices have been developed to detect a wide range of metal ions with high selectivity and sensitivity[83]. The electrochemical switches based on DNA-cleaving DNAzymes usually involve the dissociation of double-stranded DNA constructs comprised of a DNAzyme strand and its substrate strand. Plaxco et al.

reported a DNAzyme-based electrochemical switch for Pb^{2+} detection (Figure 1-16A)[84]. The DNAzyme strand was functionalized with the redox-active reporter methylene blue and immobilized on a gold electrode via a thiol-gold linkage. The DNAzyme was then hybridized to its substrate strand, prohibiting any contact between methylene blue and the electrode. In the presence of Pb^{2+}, the substrate was cleaved and the fragments were released. Such release made the enzyme strand more flexible and shortened the distance between the redox label and the electrode, leading to a higher current signal proportional to the concentration of Pb^{2+} present.

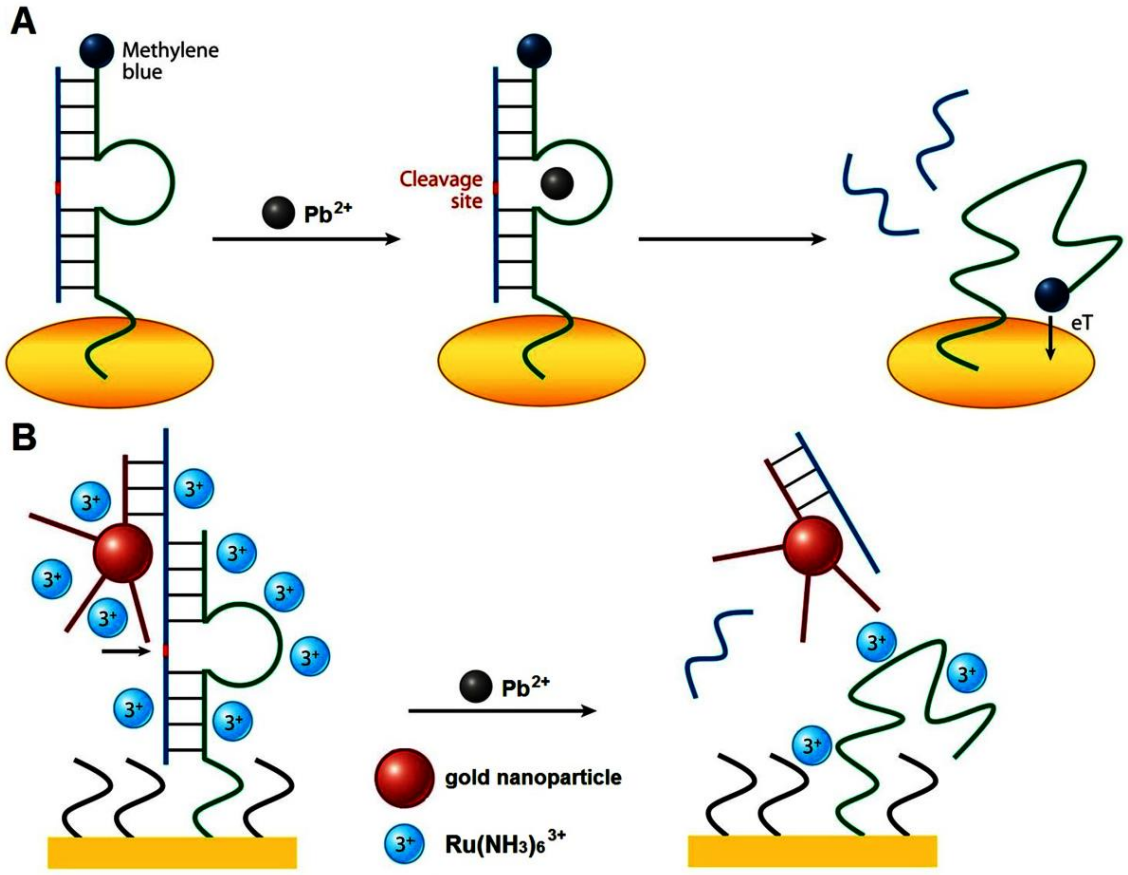

Figure 1-16. DNAzyme-based electrochemical switches for the detection of Pb^{2+} with (A) covalently tethered methylene blue and (B) solution-diffused $[Ru(NH_3)_6]^{3+}$. (A) Reprinted with permission from [84]. Copyright (2007) American Chemical Society. (B) Reprinted with permission from [87]. Copyright (2008) American Chemical Society.

A similar design for the detection of L-histidine was reported by Liang et al.[85] based on a switching structure of DNAzyme and gold nanoparticles-graphene nanosheets (GNPs-GNSs) composite. Before immobilization of the thiolated DNA duplexes, GNPs were deposited on the surface of GNSs through chemical reduction of chloroauric acid by sodium citrate; a glassy carbon electrode (GCE) was then modified with the GNPs-GNSs. The introduction of L-histidine induced self-cleavage of the DNAzyme on the GNPs-GNSs/GCE, and the redox reporter ferrocene approached the electrode surface. Because of the excellent conductivity and high surface area of graphene, the distribution of GNPs on GNSs made the fabricated switch exhibit an expanded linear range and excellent sensitivity for the detection of L-histidine.

The redox reporter at the end of the substrate strand can also be modified. Gao et al.[86] developed a DNAzyme-based switch for magnesium ion (Mg^{2+}). His system consisted of Mg^{2+}-dependent DNAzyme and a ferrocene-modified DNA substrate strand. In the absence of Mg^{2+}, the obvious faradaic current was obtained. In the presence of Mg^{2+}, the substrate was cleaved and removed resulting in a reduction of the faradaic current. The current intensity decreased with increasing Mg^{2+} concentration, permitting a quantitative determination of the Mg^{2+} concentration.

Shen et al.[87] employed short oligonucleotides functionalized with gold nanoparticles to improve the sensitivity of the DNAzyme-based switch for the detection of Pb^{2+} (Figure 1-16B). The DNAzyme hybridizes to the partially complementary substrate strand which also hybridizes to a short DNA strand with a gold nanoparticle. Because each nanoparticle carries a large number of short DNA strands which can bind to the redox reporter $[Ru(NH_3)_6]^{3+}$, more $[Ru(NH_3)_6]^{3+}$ cations bind to the DNA construct on the surface, and a higher electrochemical signal is obtained before Pb^{2+} is added. Upon binding Pb^{2+}, the DNAzyme catalyzes the hydrolytic cleavage of the substrate strand, resulting in its removal (along with the short DNA strands) from the electrode surface, fewer $[Ru(NH_3)_6]^{3+}$ cations confined on the electrode surface, and a lower electrochemical signal. The surface may be regenerated by hybridization after the substrate cleavage, allowing multiple switching cycles.

1.4.3. Quadruplex formation

The formation of unique G-quadruplex or i-motif quadruplex structures for G-rich or C-rich sequences is employed in the design of DNA-based conformational switches. Switches containing the anti-thrombin aptamer are not included in this section. Lin and co-workers[88] developed a DNA conformational switch from G-rich hairpin DNA induced by Pb^{2+}. Upon the incubation of Pb^{2+}, the G-rich hairpin DNA opens the stem-loop and forms a G-quadruplex structure, which gives rise to a sharp increase in the electron transfer resistance studied by electrochemical impedance spectroscopy (EIS) in the presence of $[Fe(CN)_6]^{3-/4-}$ as redox reporter. Shin et al.[89] reported pH induced conformational changes of an i-motif DNA nanomachine attached to single-walled carbon nanotubes (SWNTs). With increasing pH, the protonated cytosines of the i-motif are deprotonated and the DNA strand adopts a random coil structure. Cyclic voltammetry also indicated that the electrochemical signal decreases at the SWNT/DNA hybrid-modified glassy carbon electrode. Oscillating the pH between 5 and 8 resulted in reversible switching demonstrating its potential application as switchable pH-controlled electrode with switchable redox activity.

A G-quadruplex can be stabilized by coordination with specific metal ions, such as K^+ or Sr^{2+} ions, which bind between successive G-quartets. We described a contractile DNA nanoswitch[90,91] which switched repeatedly between “off” (an extended duplex) and “on” (a G-quadruplex) without dissociation of one strand and duplex regeneration by hybridization. The transition between duplex and G-quadruplex was controlled by the addition and removal of K^+ ions (Figure 1-17A). The electrochemical properties of a ferrocene-labeled DNA nanoswitch immobilized on gold were investigated by square wave voltammetry (SWV). After treatment with K^+ ions, G-quadruplex formation gave rise to a much higher oxidation current. The subsequent addition of a potassium chelator ([18]crown-6) reversed the contraction induced by the K^+ ions and restored the signal to its original low level. Reversible extension and contraction of the contractile DNA nanoswitch can therefore be repeatedly realized at a solid-liquid interface, and monitored by electronic measurements (Figure 1-17B).

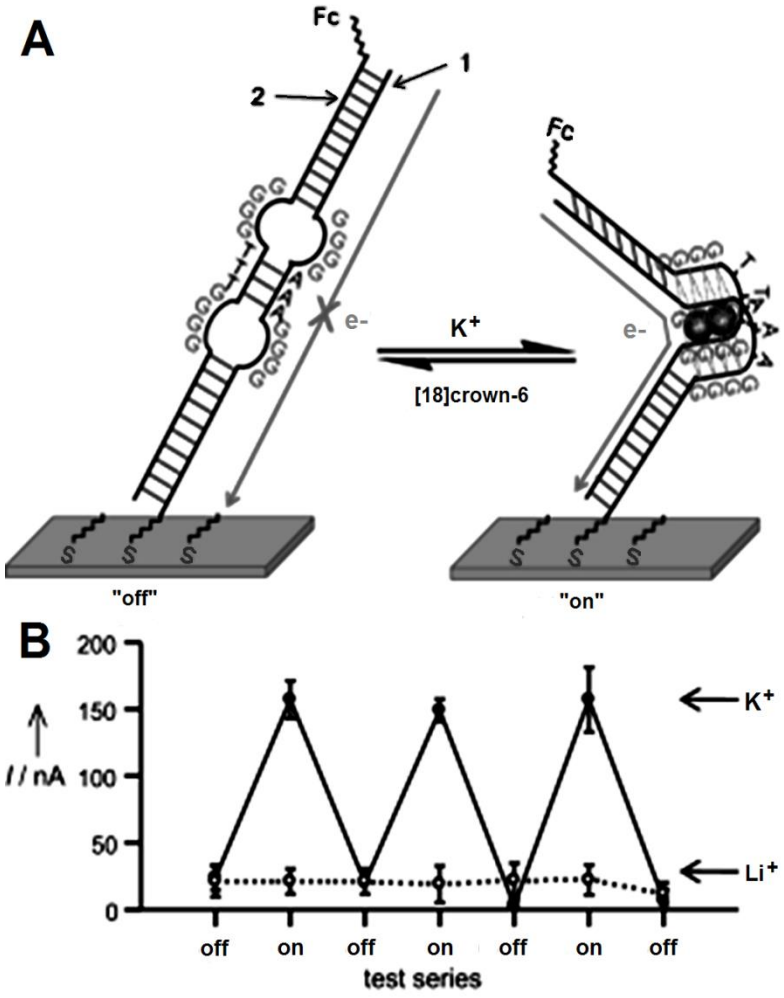

Figure 1-17. (A) A contractile DNA nanoswitch between a structurally extended "off" state (a duplex) and a contracted "on" state (a G-quadruplex) on gold controlled by the addition and removal of K^+ ions. (B) Repeated switching between the "on" and "off" states. Solid line shows the addition and removal of K^+ ions, and dashed line shows the treatment of Li^+ ions as negative control. Copyright (2010) WILEY-VCH Verlag GmbH & Co. KGaA, Weinheim. Reproduced with permission from reference [91].

1.5. Signal-switching mechanisms of DNA-based electrochemical switches

The observed signal switching induced by functional DNA is believed to be mainly due to three factors: change of the DNA-mediated electron transfer, of the distance between redox reporter and the electrode surface, and of electrostatic interactions.

1.5.1. Change of the DNA-mediated electron transfer

Barton et al.[58-60] have reported that electrons transfer through continuous base stacks of DNA, and that any perturbations such as mismatches will decrease the overall charge passed. Therefore, the introduction or removal of perturbations is one of the causes of signal switching. The ability of DNA to mediate electron transfer is taken advantage to detect even a single-base mismatch. When the base pair stack is intact, current can flow between redox reporter and electrode surface. A single-base mismatch decreases the current significantly (Figure 1-18).

The contractile DNA nanoswitch we reported[91] undergoes a conformational transition between duplex and G-quadruplex and its signal switching is due to the change of DNA-mediated electron transfer. In the absence of K^+ ions, electron transfer from ferrocene to gold through the contractile DNA switch is interrupted by the G/G mismatches and the intervening three consecutive A-T pairs, resulting in a very low electrochemical signal. Formation of the more conductive G-quadruplex from the G/G motifs on treatment with K^+ ions promotes electron transfer and gives rise to a much higher signal.

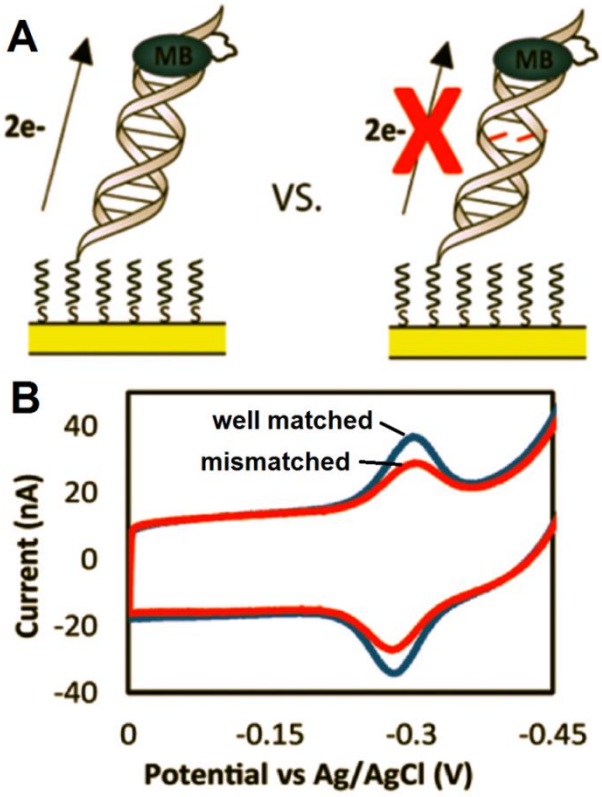

Figure 1-18. (A) Schematic representations and (B) cyclic voltammograms acquired at 100 mV/s for a well-matched DNA sequence and a sequence containing a single mismatch on gold surface. Reprinted with permission from [58]. Copyright (2012) American Chemical Society.

1.5.2. Redox-to-surface distance change

In most functional DNA-based electrochemical switches, the distance between the redox reporter (attached at the end of the DNA probe) and the electrode surface is of key importance for signal transduction. Plaxco et al.[80,81,84] have reported that when it is short, the redox reporter can be reduced directly at the surface and electron transfer is facilitated leading to a high rate constant and electrochemical signal. Anne et al.[92,93] have shown that DNA flexibility is related to redox-to-surface distance and electron transfer rate. Since single-stranded DNA is more flexible than double-stranded DNA, double-stranded DNA-based switches often dissociate first to more flexible single strand leading to a short redox-to-surface distance. Barton et al.[58] recently reported direct

reduction of a redox reporter modified at the distal end of double-stranded DNA on gold at low DNA surface density.

1.5.3. Variation of electrostatic interactions

It is known that the DNA phosphate backbone has negative charges which interact electrostatically with solution-diffused ions. The negative charges on the electrode surface can be diminished by binding to positively charged proteins[62,65] or dissociation of DNA strands[71-73]. The electrostatic repulsion between DNA and anions like $[Fe(CN)_6]^{3-/4-}$ ions is reduced because of less negative charge on the surface resulting in a higher electron transfer resistance by electrochemical impedance. Electrostatic attraction binds cations like $[Ru(NH_3)_6]^{3+}$ to the DNA on the surface. Thus, the amount of $[Ru(NH_3)_6]^{3+}$ cations measured by cyclic voltammetry (CV) reflects the amount of negative charge on DNA.

1.6. Objectives of this thesis

In 2008 we constructed a DNA device by incorporating a ferrocene-modified triple-stem DNA construct with an aptamer domain; it was then immobilized onto a gold surface and used as an ultra-sensitive electronic biosensor[94] (Figure 1-19). The design was based on our earlier electrophoretic gel shift assay study of aptamer-containing DNA constructs[95]. Two different designs were tested successfully (Figure 1-20). In particular, an “integrated-ligand” DNA switch was constructed by incorporating an aptamer domain in the middle of an otherwise complementary DNA duplex. Compared to biochemical analysis of guanine damage within the DNA, an electrochemical approach would be more valuable for probing electron transfer through DNA.

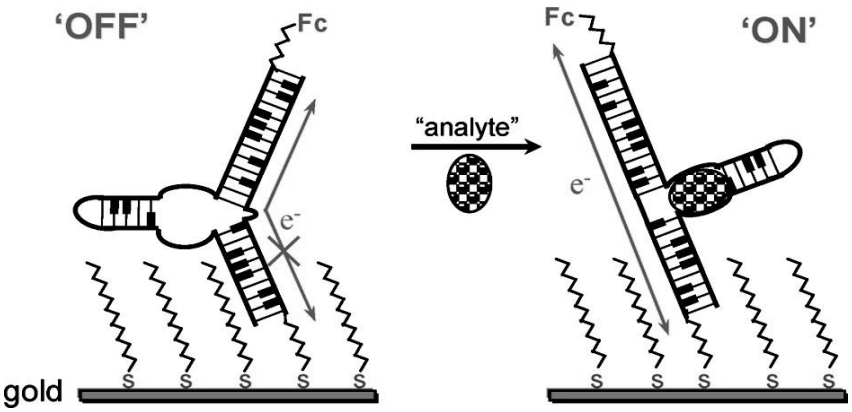

Figure 1-19. Schematic representation of an ultra-sensitive electronic biosensor by immobilizing a ferrocene(Fc)-modified triple-stem DNA construct onto a gold chip. Reprinted with permission from [94]. Copyright (2008) American Chemical Society.

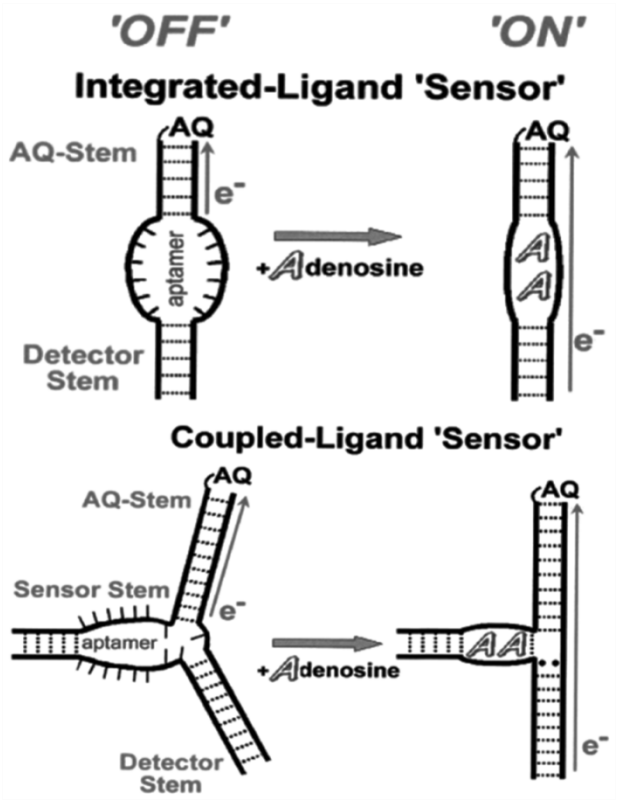

Figure 1-20. Design of an "integrated-ligand" and a "coupled-ligand" DNA switch. Reprinted with permission from [95]. Copyright (2002) American Chemical Society.

In this thesis, we report the construction and testing of a new version of an integrated-ligand DNA switch labeled with methylene blue (MB) on its distal end and immobilized onto a gold surface. In prior work, MB covalently tethered to DNA through a short alkyl linkage has been shown to be a successful redox moiety for this platform which couples to the DNA's base stack through intercalation[58,96]. Our integrated-ligand DNA switch incorporates an adenosine-binding DNA aptamer. NMR studies have shown that the binding of two adenosine ligands to the aptamer leads to the formation of six contiguous hydrogen-bonded and stacked base mismatches[67]. The tertiary structure determined by NMR and molecular dynamics calculations indicated that the perturbations in base stacking were repaired to some extent and the flexibility of whole DNA construct was also reduced. Therefore, the deliberate removal of perturbations or a change in surface accessibility of the redox reporter are both possibly responsible for the signal switching of the designed DNA switch. The extent to which each mechanism contributes to the observed signal was found to be directly influenced by assembly conditions[58]. In principle, we can differentiate which mechanism is dominating under any given assembly condition by examining the redox signal dependence on π-stack perturbations including the determination of electron transfer rates[97,98].

In this work, the "integrated-ligand" DNA-aptamer construct at various surface densities was investigated in the absence or presence of adenosine to evaluate the functioning of such a DNA switch. A unique "bipolar" switching performance was observed that is distinct from the usual one-way DNA nanoswitch[91]. More importantly, we found that neither of the above two mechanisms were responsible for the signal switching in our DNA switch. In fact, the lateral intermolecular interaction between the end-tethered redox centers is the main contributing factor to the signal switching. Based on Laviron's theories on surface electrochemical reaction of strongly adsorbed systems and of redox modified electrodes[99], the variation of intermolecular interactions was modeled before and after binding adenosine. The agreement between the experimental and theoretical results confirms the proposed intermolecular interaction-dictated redox switching mechanism.

2. Experimental Section

2.1. Materials

The HPLC-purified doubly modified and unmodified DNA oligonucleotides were purchased from Biosearch Technologies (Novato, CA). Three sequences were used to prepare the DNA switch and the fully complementary duplex (control construct). Strands 1 and 2 were used to construct the switch (MB-SWITCH-SH) and strands 1 and 3 were used to prepare the fully complementary duplex as negative control (MB-COMP-SH). Underlined bold bases in strands 1 and 2 form the 12-base mismatch loop which bind two adenosine molecules in the DNA switch. Also, a thiol-modified strand 1 without MB tag was obtained from Biosearch Technologies and used to dilute the concentration of MB in DNA monolayers at similar surface densities. The sequences of the three strands are as follows:

Strand 1 (MB and thiol-modified DNA): 5'-[MB-(NH-C_6-acrylamido-T)]-ATC AAG GT**<u>G GGG GA</u>**T GGC TAA A-[O-$(CH_2)_6$-S-S-$(CH_2)_6$-OH]-3'

Strand 2: 5'-TTT AGC CA**<u>G GAG GA</u>**A CCT TGA T-3'

Strand 3: 5'-TTT AGC CAT CCC CCA CCT TGA T-3'

Gold substrates (regular glass slides first coated with 5-nm Cr, followed by 100-nm Au) were purchased from Evaporated Metal Films Inc. (Ithaca, NY). Tris-(2-carboxyethyl)phosphine hydrochloride (TCEP), 6-mercapto-1-hexanol (MCH) and hexaammineruthenium (III) chloride (98%) were used as received from Sigma-Aldrich (St. Louis, MO). All solutions were made with deionized water (>18.3 MΩ•cm) from a Barnstead EasyPure UV/UF compact water system (Dubuque, IA).

2.2. Gel electrophoresis

The formation of the structures of the DNA switch and of the duplex control was confirmed by gel electrophoresis. The DNA was suspended in standard buffer (10 mM Tris, 150 mM LiCl, 3 mM $MgCl_2$ at pH 7.4) and the final concentration was 2.0 µM. The 14% non-denaturing gel was run to compare the formation and mobility of the DNA constructs before and after adding adenosine for both the DNA switch and the duplex control. A 19:1 acrylamide / bisacrylamide solution was used as stock solution. The loading volume of each individual lane was 10 µL. The gel was run in a SE600 Series Standard Vertical Electrophoresis Unit at 300 V for 2.5 hours. The gel-loading dye contained Bromophenol Blue and Xylene Cyanol FF to track the position of the DNA strands on the gel. After running the gel was stained overnight with ‘‘stains-all” solution and de-stained before reading.

2.3. DNA immobilization on gold

The disulfide bond of strand 1 (the thiolated DNA) was reduced with 10 mM TCEP in 100 mM Tris buffer at pH 7.4 for 4 h, followed by desalting with a MicroSpin G-25 column (GE Healthcare, UK) according to the manufacturer’s instructions. The columns were equilibrated with deoxygenated standard buffer (10 mM Tris, 150 mM LiCl, 3 mM $MgCl_2$, pH 7.4) prior to use. The resulting thiol-terminated strand 1 was then hybridized with strand 2 or 3 in standard buffer by incubating at 80 °C for 2 min, followed by slow cooling to room temperature over a period of 60 min to form MB-SWITCH-SH (strands 1 and 2) or MB-COMP-SH (strands 1 and 3).

The gold slides were cleaned by immersion in a freshly prepared “piranha” solution (3:1 mixture of concentrated H_2SO_4 and 30% H_2O_2) at 90 °C for 5 min (*WARNING: piranha solution reacts violently with organic solvents*), rinsed thoroughly with deionized water and dried under N_2. Freshly prepared MB-SWITCH-SH and MB-COMP-SH were then immobilized on the clean gold surface by spreading a 15-µL droplet and then stored at 100% humidity at room temperature for 12-24 h. After immobilization, the gold slides were rinsed with standard buffer three times, followed by incubation in 1 mM MCH in the same buffer for 1 h to minimize nonspecific DNA

adsorption on the surface. The gold slides were rinsed again and incubated with standard buffer, and then stored at 100% humidity before electrochemical characterization.

2.4. Electrochemical measurements

A CHI660D series potentiostat/galvanostat electrochemical workstation (CH Instruments, Austin, TX) was used to perform electrochemical experiments with a 1-mL three-electrode cell. A DNA-modified gold chip was used as working electrode (with a geometric area of 0.126 cm^2), Ag | AgCl | 3 M NaCl as reference electrode and a curling platinum wire as counter electrode. Cyclic voltammetry (CV) and square wave voltammetry (SWV) measurements were carried out at different concentrations of adenosine in 10 mM Tris, 150 mM LiCl, 3 mM $MgCl_2$ at pH 7.4 to investigate the redox reaction of MB tagged on DNA constructs. The DNA surface density on gold was measured with the charge integrated from the reduction peak of 5.0 μM $[Ru(NH_3)_6]Cl_3$ in 10 mM Tris buffer at pH 7.4 (degassed with argon for at least 15 min).

3. Results and Discussion

3.1. Switching properties of the DNA switch

3.1.1. DNA switch design

The DNA switch (MB-SWITCH-SH) contains a 12-oligonucleotide internal loop, the anti-adenosine aptamer sequence in the middle of an otherwise complementary DNA double helix (Figure 3-1A). Methylene blue (MB) was covalently tethered to the 5'-terminus of strand 1 as the redox marker. The 3'-end of strand 1 was modified with a thiol group, enabling the formation of robust DNA self-assembled monolayers on a gold electrode via sulfur-gold linkages. The anti-adenosine aptamer containing DNA construct (MB-SWITCH-SH) was formed by hybridization of strands 1 and 2, with a relatively unstructured loop (12 mismatched bases) in the middle. A complete Watson-Crick base-paired double helix (MB-COMP-SH) formed by strand 1 and its fully complementary strand 3 was used as control after immobilization on a gold surface (Figure 3-1C).

Upon adding adenosine to the electrolyte, two adenosine molecules will bind to the internal loop of the DNA switch (Figure 3-1B). The internal bulge of the DNA aptamer "zips" up through formation of a continuous six-base mismatch segment[67]. The adenosine molecules pair via their Watson-Crick edges with the minor groove edges of guanine residues. Long et al. have suggested that electron transport through an intra- rather than an inter-strand pathway is more favorable[100]. Therefore the redox center MB was tethered at the 5' terminus of strand 1, and the 3'-end was modified with a thiol group in our design. It is crucial to examine whether the structural rearrangement induced by adenosine binding to the aptamer domain would have any influence on the MB redox properties.

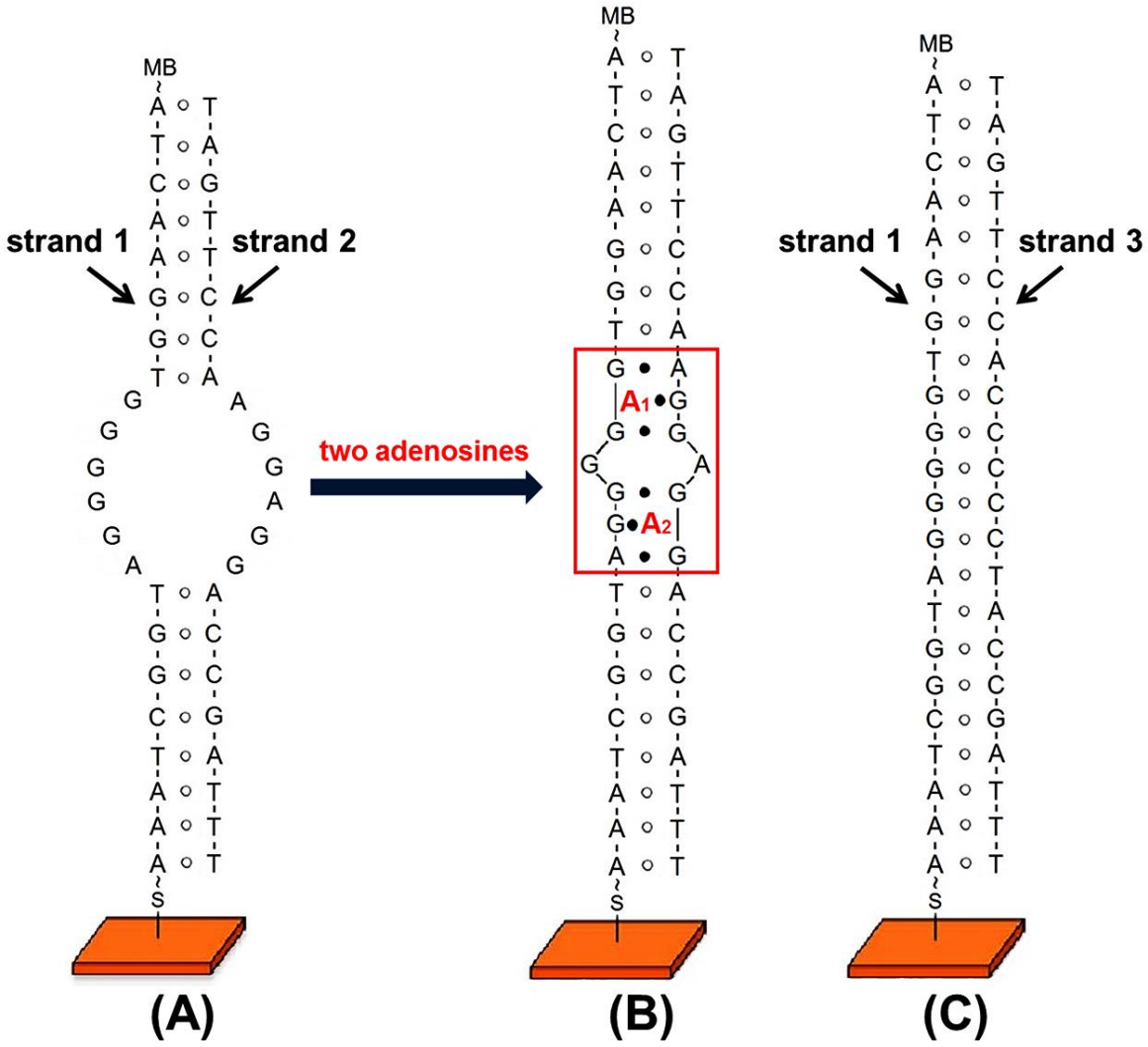

Figure 3-1. Design of DNA switches on electrodes. (A) DNA switch (MB-SWITCH-SH) formed by strands 1 and 2 has a 12-oligonucleotide internal bulge (the anti-adenosine aptamer sequence). Strand 1 is modified with the redox marker methylene blue (MB) at its 5' terminus and with a thiol linker at its 3' terminus. (B) Upon binding two adenosine molecules (red letters A_1 and A_2), six consecutive base mismatches are formed in the bulge (red rectangle). The six black circles represent the non-Watson-Crick base mismatches. (C) Fully complementary DNA duplex without aptamer sequence (MB-COMP-SH) is formed by strands 1 and 3 as control. The open circles represent the Watson-Crick base pairs formed between DNA strands.

The assembly and integrity of the DNA switch and of the duplex control were confirmed in solution using gel electrophoretic assays. As shown in Figure 3-2, the incubation of 1.0 mM adenosine with the DNA switch (Lane 6) shows a slightly faster mobility compared to the construct without adenosine (Lane 5), indicative of a conformational change of the switch. We have not observed any breakdown of the structure after adenosine binding; neither have we observed any upper bands which could possibly form through base stacking of multiple units.

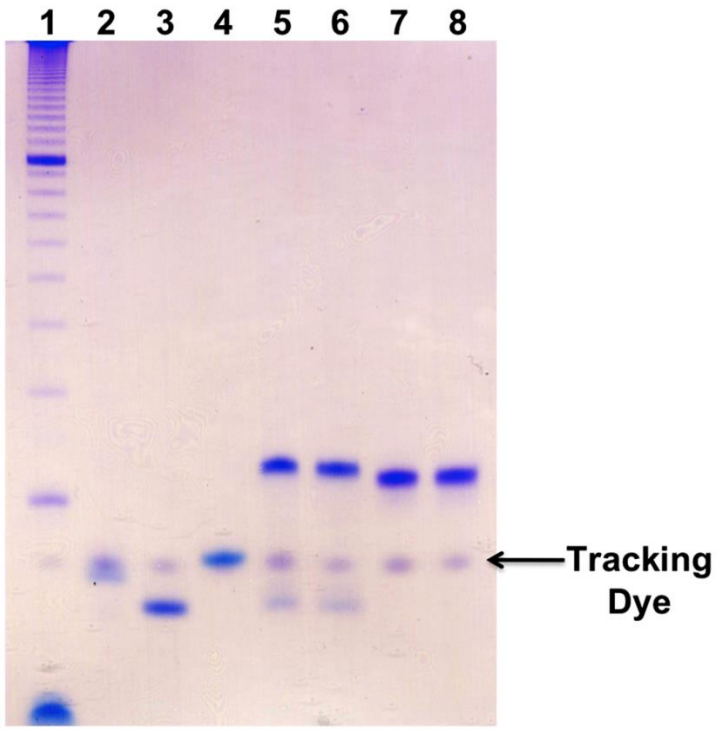

Figure 3-2. Gel electrophoresis analysis of the formation of the DNA switch and of the fully complementary control duplex. Lane 1: 10 base-pair ladder marker. Lane 2: strand 1 (thiolated DNA with 22 nucleotides). Lane 3: strand 2 (aptamer strand of 22 nucleotides). Lane 4: strand 3 (complementary DNA of strand 1 of 22 nucleotides); lane 5: DNA switch formed by partial hybridization of strands 1 and 2. Lane 6: incubation of DNA switch with 1.0 mM adenosine overnight. Lane 7: control duplex formed by complete hybridization of strands 1 and 3. Lane 8: incubation of the control duplex with 1.0 mM adenosine overnight.

3.1.2. Effect of surface density

The surface density of DNA constructs on a gold surface is an important factor affecting the performance of the DNA switch[101]; we have controlled the surface density by changing the concentration of preformed DNA constructs in the deposition solution during the preparation step. The DNA surface density was first determined by measuring the integrated charge (peak area) of the MB reduction peak in cyclic voltammetry (CV) experiments. The relationship between the total charge (Q, in coulombs) and the surface density of the MB moiety (Γ) is described as,

$$Q = nFA\Gamma \qquad \text{(Equation 3-1)}$$

where n is the number of electrons transferred per MB moiety (n=2), A is the electrode surface area, and F is the Faraday constant.

By controlling the DNA concentration in the deposition solution as well as the assembly time, we were able to fabricate DNA switch-modified gold electrodes with surface densities ranging from 1.1×10^{12} to 1.2×10^{13} molecules/cm^2. We found that, in the presence of adenosine, different trends of signal changes were obtained upon varying the surface density of the immobilized DNA constructs. At a high surface density (1.0×10^{13} molecules/cm^2, Figure 3-3A), there was no significant variation in the integrated charge (peak area) of MB reduction upon adding 1.0 mM adenosine into the electrolyte (*vide infra*); rather, the reduction peak became narrower and higher at MB-SWITCH-SH-modified electrodes. The observation of a linear relationship between peak current and scan rate before and after adding adenosine indicates a surface-bound redox process (Figure 3-4). The equilibration time was short and the reduction current reached the maximum in less than 5 min. When the DNA surface density was decreased to 6.0×10^{12} molecules/cm^2 (Figure 3-3B), a similar response was obtained except the peak current increase was smaller than that at higher surface density. However, when continuing to reduce DNA surface density to 2.0×10^{12} molecules/cm^2 (Figure 3-3C), the reduction peak became broader for the DNA switch after adding adenosine with no significant change in the peak area. Compared to the MB-SWITCH-SH-modified electrodes, there was no signal change at MB-COMP-SH-modified electrodes with varying DNA surface densities upon adding 1.0 mM adenosine (Figure 3-3D-F).

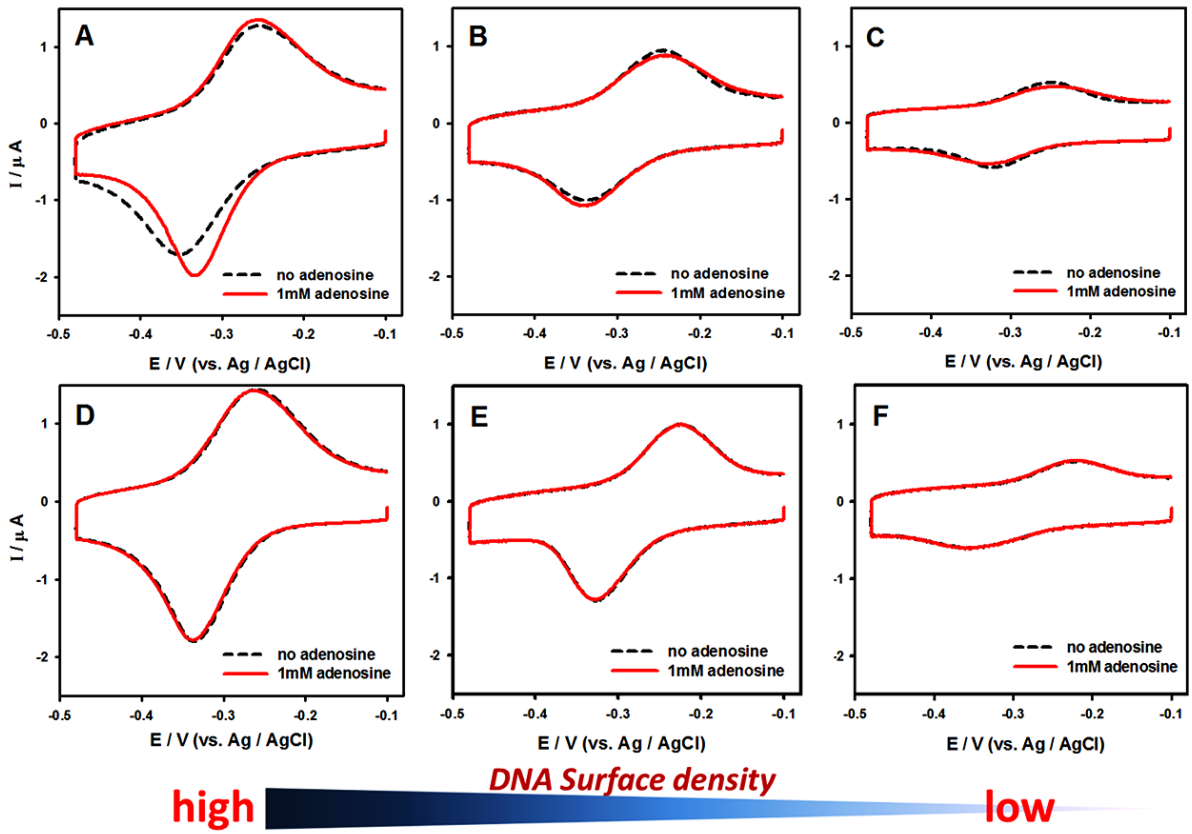

Figure 3-3. Comparison of the electrochemical responses of the DNA switch and the control system at varying surface densities. CV was performed before (black dash line) and after (red solid line) adding 1.0 mM adenosine in standard buffer (A-C) at MB-SWITCH-SH-modified electrodes and (D-F) at MB-COMP-SH-modified electrodes. The DNA surface densities calculated from the integrated charge (peak area) of MB reduction (Γ_{DNA}) for (A, D), (B, E), and (C, F) were 1.0×10^{13}, 6.0×10^{12}, and 2.0×10^{12} molecules/cm^2, respectively. The scan rate of all CVs was 300 mV/s.

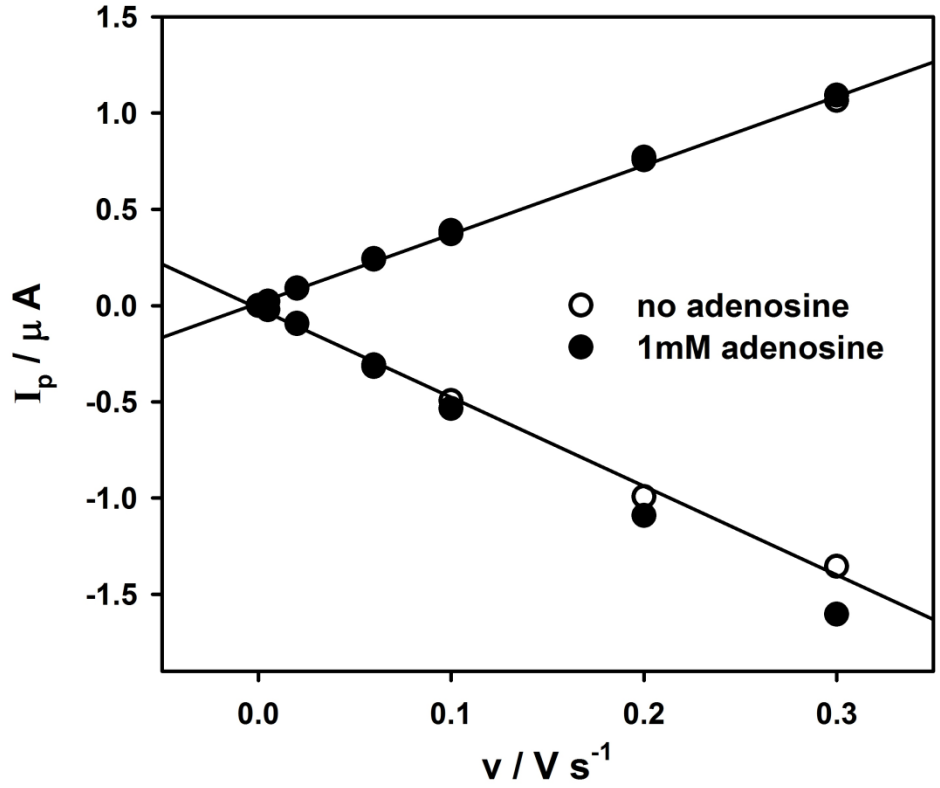

Figure 3-4. The CV peak current during MB oxidation and reduction as function of scan rate before and after adding 1.0 mM adenosine at a high-density MB-SWITCH-SH-modified electrod. Γ_{DNA} was 1.0×10^{13} molecules/cm^2.

To better illustrate the influence of surface density on redox switching, the relative reduction peak current change ($\Delta I/I$) upon binding adenosine is summarized in Figure 3-5. It is clear that at high surface densities (> 4.1×10^{12} molecules/cm^2), the reduction peak current increases after adding adenosine; but at low surface densities (< 4.1×10^{12} molecules/cm^2), the peak current intensity decreases upon ligand binding. This means that the DNA construct exhibits a "bipolar" switching behavior in response to adenosine binding upon varying the surface packing density. But no change is observed in the control system (the duplex, Figure 3-1C), which confirms that the "bipolar" switching behavior results from adenosine binding to the aptamer domain of the DNA switch. In addition, it is worthy to note that at all surface densities the mean distance between neighboring DNA molecules is less than twice the DNA length.

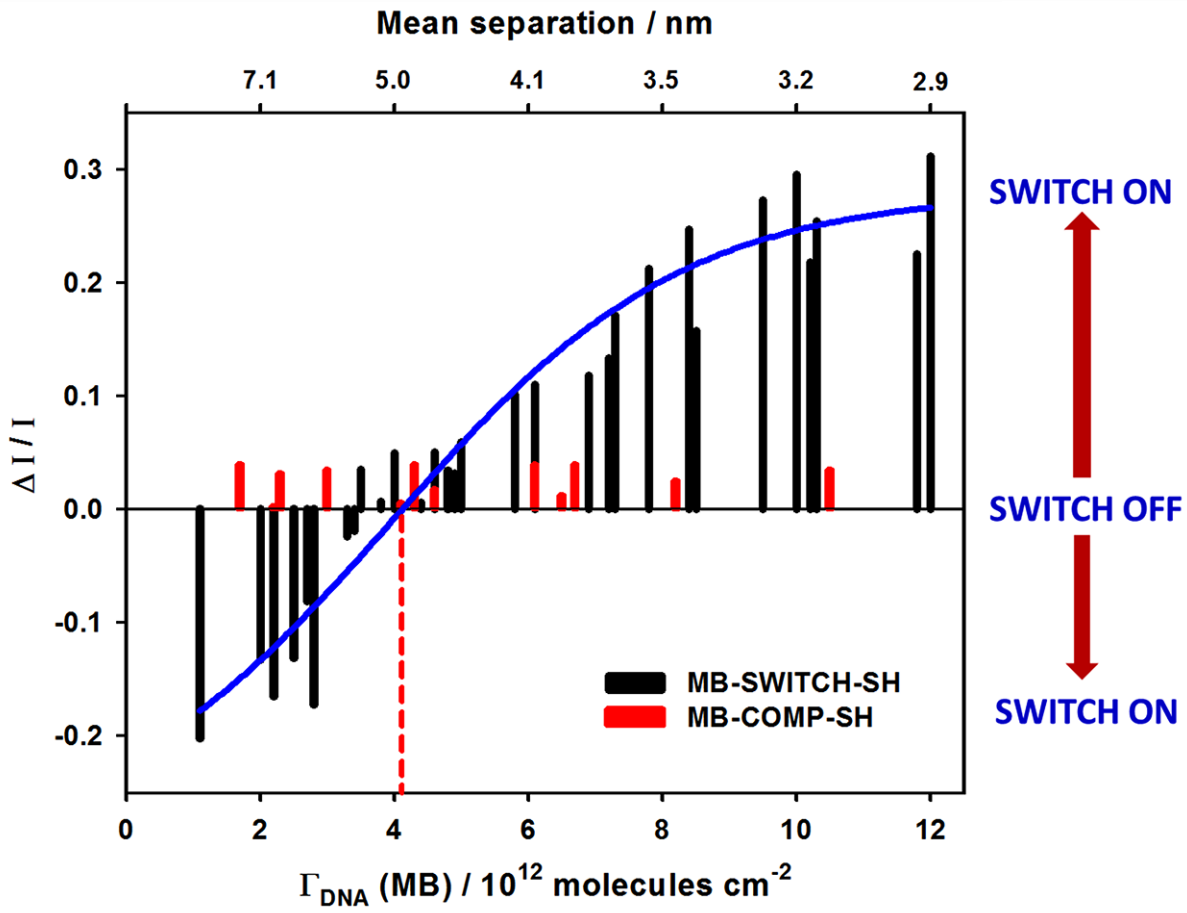

Figure 3-5. Relative CV peak current change (Δ*I*/*I*) during MB reduction upon binding adenosine as function of DNA surface density (Γ_{DNA}) for MB-SWITCH-SH (black columns) and MB-COMP-SH (red columns) modified gold electrodes, respectively. The blue curve is the best fit to the data for MB-SWITCH-SH-modified electrodes. There is no current change at the surface density of 4.1±0.3×10^{12} molecules/cm^2.

3.1.3. Specificity, reusability and stability

The switching behavior of the DNA switch after adding different concentrations of adenosine was investigated by the above CV measurements and the relative cathodic peak current change (ΔI/I) was plotted as a function of adenosine concentration. Figure 3-6A shows the binding isotherm of adenosine at the MB-SWITCH-SH-modified electrode. The surface dissociation constant of the adenosine-DNA-switch complex (K_d) was 40±3 μM, and the minimum concentration of adenosine needed to generate a

visible redox signal change was 15 μM. For practical applications, square wave voltammetry (SWV) is often used because of its high signal-to-noise ratio and resolution[102]. The signal change of SWV for the same concentration of adenosine was higher than that of CV at MB-SWITCH-SH-modified electrodes (Figure 3-7). However, the uncertainty for the calculation of integrated charge in SWV was too large to obtain accurate surface densities[103]. Therefore, only the integrated charge obtained from CV curves was used to calculate the DNA surface density in this study.

To demonstrate the specificity of adenosine binding, the DNA switch was challenged with analogue molecules such as uridine monophosphate (UMP) and guanosine monophosphate (GMP), as well as with adenosine monophosphate (AMP) and adenosine-5'-triphosphate (ATP) which "share" the same aptamer sequence with adenosine. Figure 3-6B compares the CV responses of our DNA switch treated with adenosine, UMP, AMP, GMP, and ATP at the same concentration of 1.0 mM. It is clear that at both high and low surface densities, the DNA switch did not respond to UMP or GMP but it did respond to AMP and ATP. The binding of AMP or ATP induces the same "bipolar" switching at varying surface densities as does adenosine. The fact that the DNA switch binds ATP, AMP, and adenosine with similar affinity (Figure 3-6B) suggests that the negatively charged phosphate moiety does not interact strongly with the aptamer, i.e., it may be oriented away from the DNA backbone[66]. The reason that ATP showed a smaller signal change than adenosine and AMP at high surface densities may also be due to its significant steric effects when "passing" through the packed DNA monolayer (see the chemical structures of adenosine, AMP and ATP in Figure 3-8). The similar signal change for adenosine, AMP and ATP at low surface densities also supports the above argument, i.e., there are no discernible steric effects when the distances between DNA switches are large enough. To enhance the selectivity of DNA switch, another aptamer sequence could be selected with specific binding to adenosine only, not AMP and ATP. A counter selection with AMP and ATP may be employed in the process of selection.

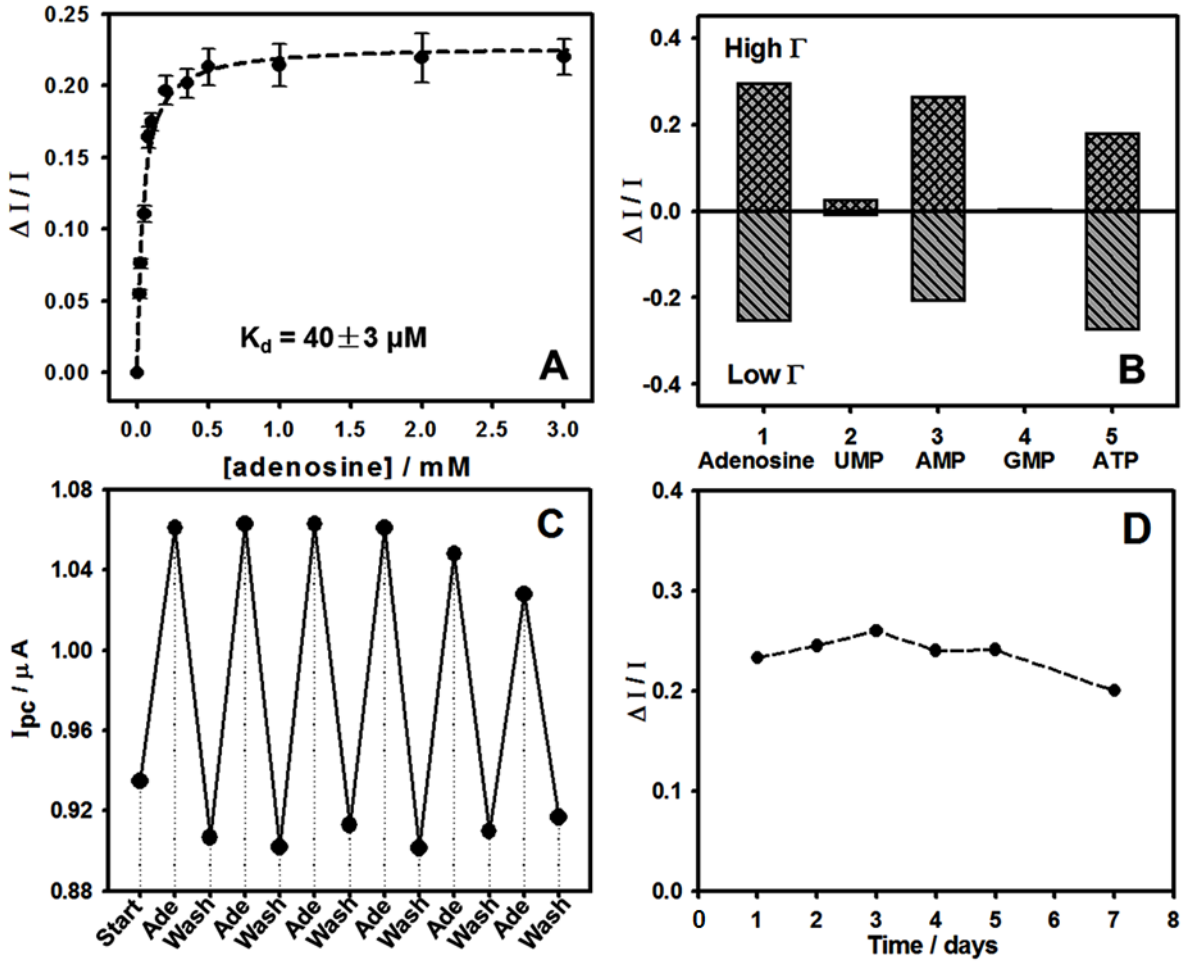

Figure 3-6. (A) Relative CV peak current change (Δ*I*/*I*) during MB reduction as function of adenosine concentration (in mM) at an MB-SWITCH-SH-modified electrode. Γ_{DNA} was 8.5×10^{12} molecules/cm^2. (B) Relative CV peak current change (Δ*I*/*I*) during MB reduction at an MB-SWITCH-SH-modified electrode at high and low surface densities after incubation in 1.0 mM (1) adenosine, (2) UMP, (3) AMP, (4) GMP, and (5) ATP, respectively. Γ_{DNA} for high Γ and low Γ was 1.2×10^{13} and 1.1×10^{12} molecules/cm^2, respectively. (C) Reduction peak current for the first six cycles of adenosine binding (in 1.0 mM adenosine) and release by treatment with adenosine-free buffer. Γ_{DNA} was 7.3×10^{12} molecules/cm^2. (D) Stability of the DNA switch in the first eight days after preparation of the electrode. Γ_{DNA} was 1.0×10^{13} molecules/cm^2.

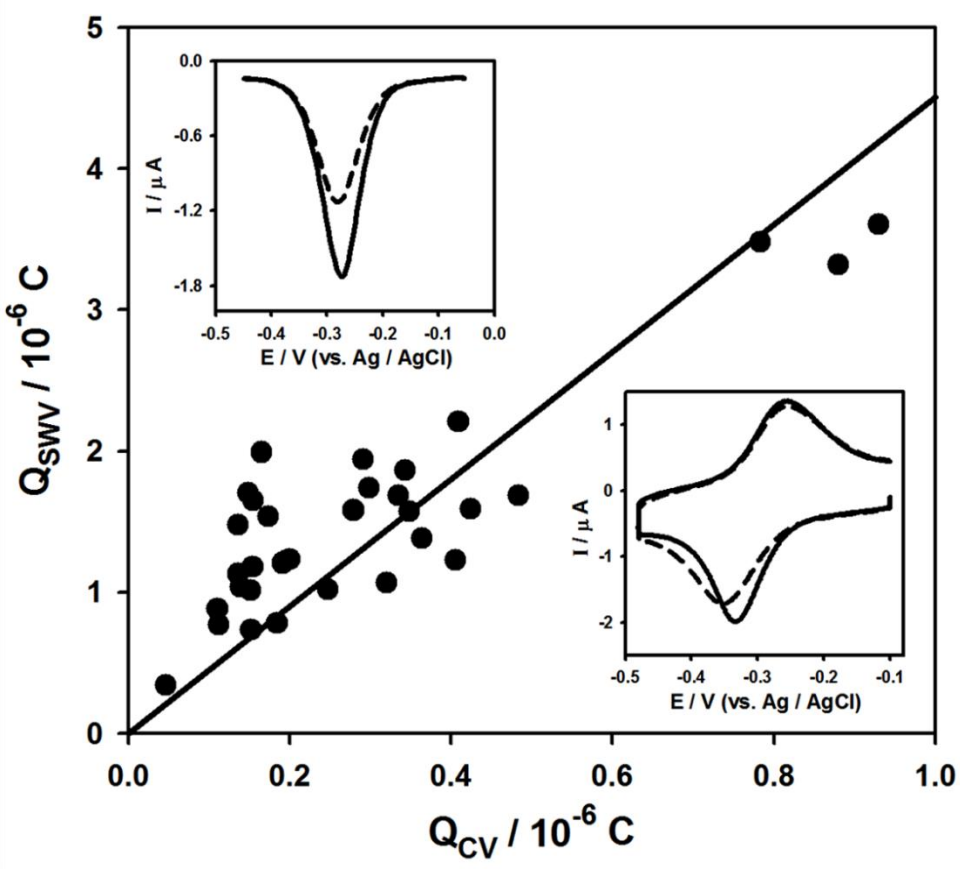

Figure 3-7. Relationship between the integrated charge (peak area) during MB reduction from CV and the one from SWV at the MB-SWITCH-SH-modified electrode. The insets show a comparison of CV and SWV signal changes before and after adding adenosine.

The chemical stability of nucleic acids ensures that the DNA switch is regenerated under conditions that may lead to dissociation of the aptamer-ligand complex. Figure 3-6C highlights the “reusability” of the DNA switch. In this experiment, the DNA switch was challenged with 1.0 mM adenosine and then regenerated by treatment with adenosine-free standard buffer. At high surface densities, the binding of adenosine made the reduction peak current increase, and the subsequent release of adenosine from DNA made the signal decrease. We have shown that the DNA switch retains significant levels of activity after six cycles of adenosine binding and release. The stability of our DNA switch was also investigated (Figure 3-6D). The response to adenosine was still as good as initially even six days after preparation of the electrode. A

small decrease in response was observed after eight days. In these experiments, the modified gold electrodes were covered with standard buffer and stored at room temperature and 100% humidity; better storage methods (e.g., O_2-free environment and at low temperature) may lead to further improvement of the stability.

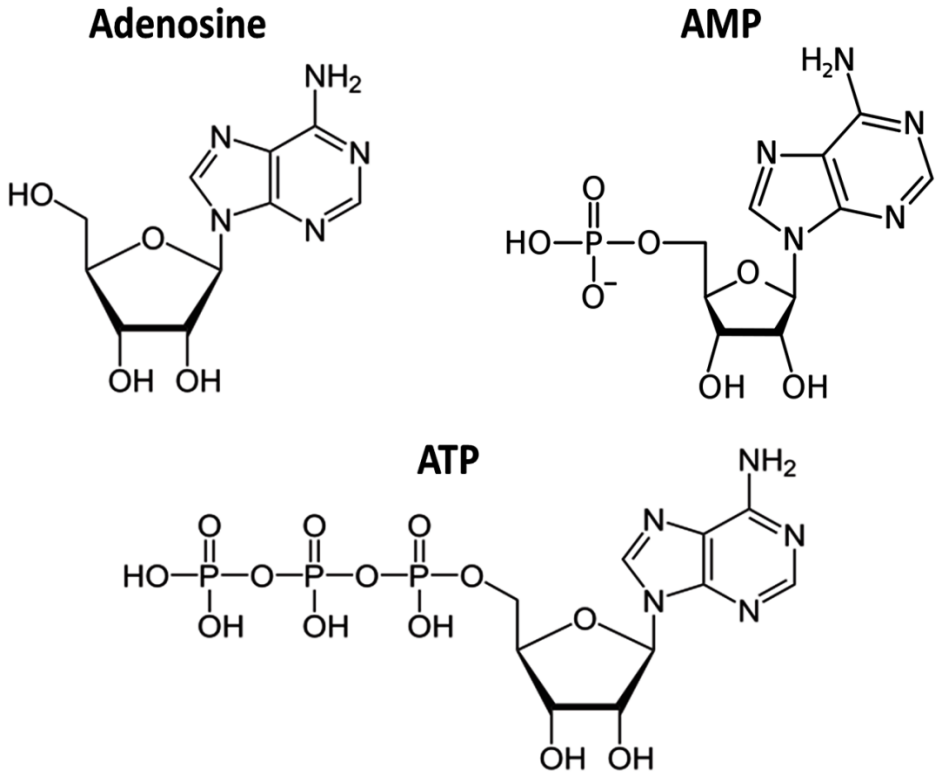

Figure 3-8. The chemical structures of adenosine, AMP and ATP.

Several versions of electrochemical biosensors have been recently designed for the detection of adenosine due to its important functions in the central nervous system and in the immune system[104-107]. Zuo et al.[69] designed a target-responsive electrochemical aptamer switch (TREAS) that functioned by switching structures from DNA/DNA duplex to DNA/target complex with ferrocene (Fc) labeling. The aptamer forms a tertiary structure with ATP which brings the Fc close to the electrode surface resulting in the signal-on state. When the leaving strand from the duplex is the aptamer strand, a signal-off sensor has been developed[70,72,74]. We do not expect these constructs to perform identically to our switch since duplex dissociation occurs when the target is

introduced. The regeneration process takes much longer time as it involves both thermal dehybridization and hybridization reactions. Du et al.[108] fabricated a microfluidic electrochemical aptamer-based sensor (MECAS) for the multiplex detection of ATP and cocaine. A second aptamer fragment must be introduced into the sensing platform together with the analyte; signal amplification with gold nanoparticles makes adaptation of this design as a switching device difficult. However, the DNA switch we designed has potential as an electronic biosensor with ease of preparation, good reusability and stability.

3.2. Switching mechanism of the DNA switch

3.2.1. Confirmation of surface density distribution

One of the key issues in the study of redox-labeled DNA constructs immobilized on an electrode surface is the electroactivity and electrochemical accessibility of the end-tethered redox moieties. To investigate this, we determined the DNA surface density by measuring the CV of DNA-modified electrodes in 5.0 μM $[Ru(NH_3)_6]^{3+}$ solution[63,64]. The integrated charge of the cathodic peak (produced by reduction of the electrostatically bound $[Ru(NH_3)_6]^{3+}$) can be used to calculate the number of DNA strands on the surface. The relationship between the surface densities calculated from MB reduction peak area and those from $[Ru(NH_3)_6]^{3+}$ experiment of the MB-SWITCH-SH-, MB-COMP-SH- and ssDNA-modified electrodes is illustrated in Figure 3-9. For the fully complementary dsDNA (MB-COMP-SH) and ssDNA, the two sets of surface densities were almost equal. It is surprising that for MB-SWITCH-S-Au the surface densities determined from $[Ru(NH_3)_6]^{3+}$ experiment were about half as large as the values obtained from the MB reduction peak area. Possible reasons for this discrepancy may be the rather weak binding of $[Ru(NH_3)_6]^{3+}$ to the relatively unstructured “loop” section of the DNA construct, or the inhibited migration of $[Ru(NH_3)_6]^{3+}$ cations into the section underneath the loop. It is also possible that the DNA-switch-modified electrodes have a mixed DNA film consisting of DNA switch and ssDNA strands.

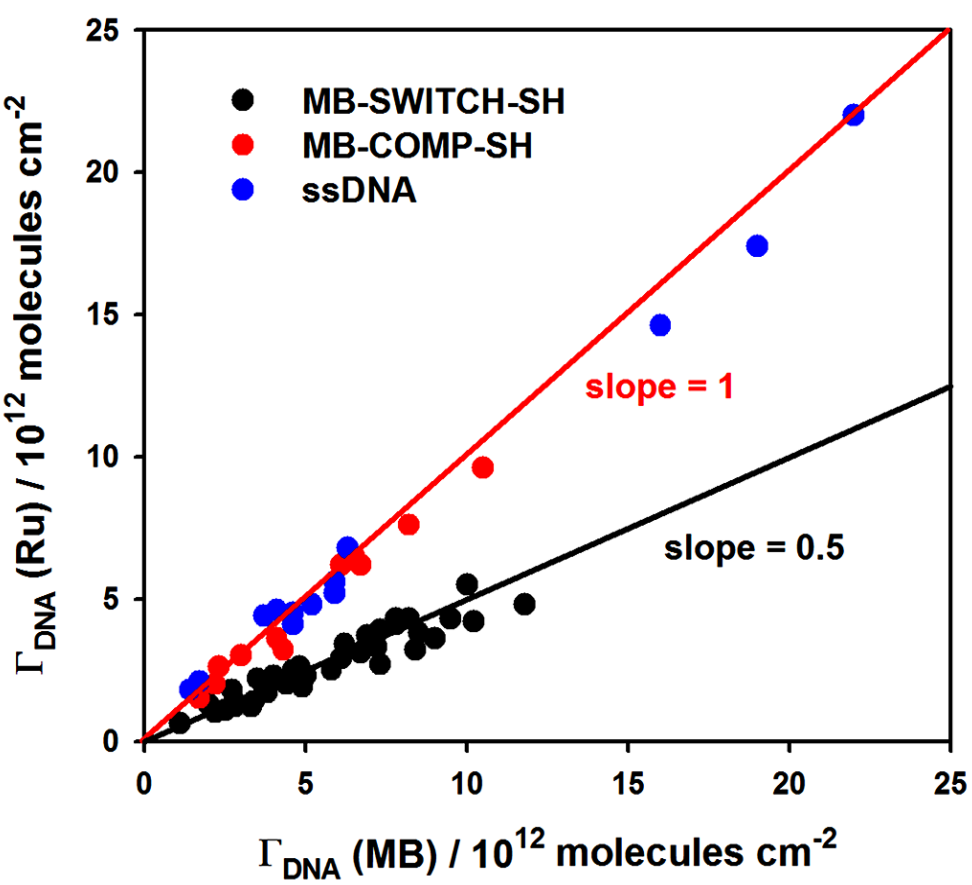

Figure 3-9. Relationship between the DNA surface densities calculated from the reduction peak of MB [Γ_{DNA}(MB)] and that of surface-bound [$Ru(NH_3)_6]^{3+}$ [Γ_{DNA}(Ru)] at the MB-SWITCH-SH- (black circles), MB-COMP-SH- (red circles), and ssDNA-(blue circles)modified electrodes. The red and black lines have slopes of 1.0 and 0.5, respectively.

As mentioned above, there was no significant variation in the integrated charge (peak area) of MB reduction upon adding 1.0 mM adenosine to the electrolyte at MB-SWITCH-SH-modified electrodes. Figure 3-10 shows the relative charge change as a function of DNA surface densities. The variation of the integrated charges (which corresponds to the number of electroactive MB molecules) before and after binding adenosine is within ±5%. Considering the surface density measurements discussed above, it is reasonable to conclude that all MB molecules in the DNA monolayer are electroactive, for both MB-COMP-SH- and MB-SWITCH-SH-modified electrodes.

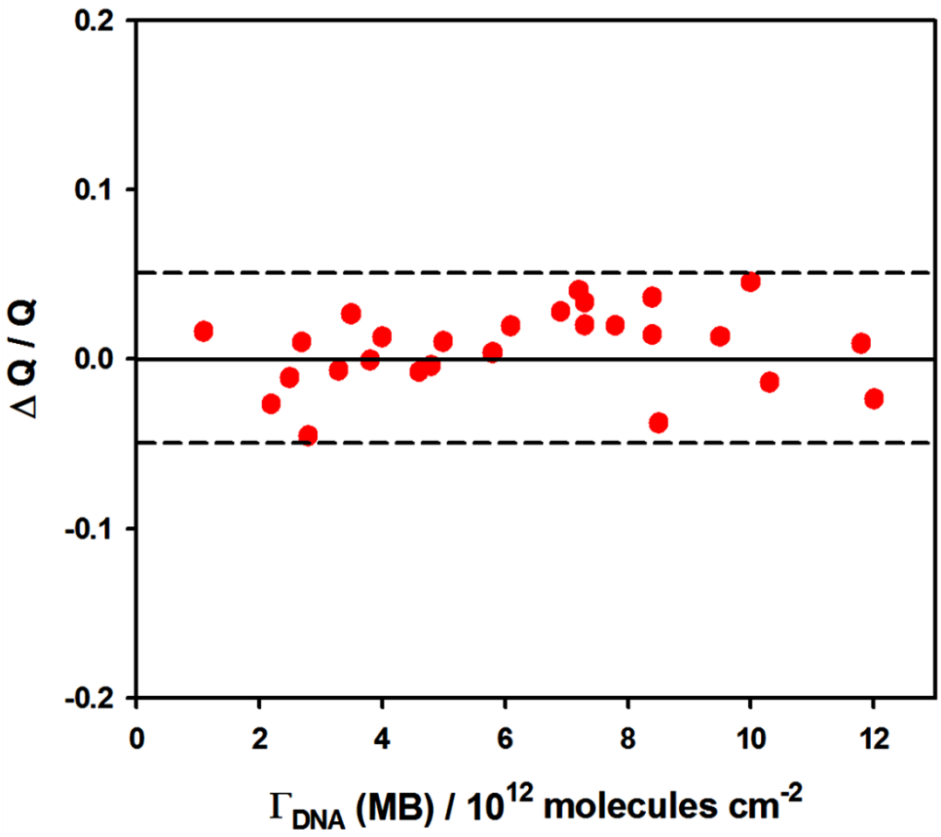

Figure 3-10. Relative integrated charge (peak area) change (ΔQ/Q) during MB reduction upon binding adenosine as function of DNA surface density (Γ_{DNA}) for MB-SWITCH-SH-modified electrodes.

3.2.2. Electron transfer kinetics

Because a change of electron transfer rate constants can lead to a change of electrochemical response (i.e., changes in CV curves), the electron transfer rate constant (*k*) was determined before and after adenosine binding at MB-SWITCH-SH-modified electrodes. The rate constant *k* of the MB redox reaction at DNA-modified gold electrodes can be readily calculated based on the Laviron classical model[109];

$$E_{pc} = E^{o'} - \frac{RT}{\alpha nF}\ln\left(\frac{\alpha nFv}{RTk}\right) \qquad \text{(Equation 3-2)}$$

$$E_{pa} = E^{o'} - \frac{RT}{(1-\alpha)nF}\ln\left(\frac{(1-\alpha)nFv}{RTk}\right) \qquad \text{(Equation 3-3)}$$

where E_{pc} and E_{pa} are the cathodic and anodic peak potentials, respectively, $E°'$ is the formal potential, n is the number of electrons transferred, and α is the transfer coefficient for the cathodic process. R, T, and F have their usual meanings. The simple analytical procedure consists of recording cyclic voltammograms at different scan rates (v) and subsequently plotting the relative peak potentials (E_p - $E°'$) versus ln v. The k and α values can be derived from an analysis of the linear section of the plot (i.e., at the higher scan rates when $\Delta E_p > 200/n$ mV).

The electron transfer rate constant k as a function of DNA surface density before and after adding adenosine at the MB-SWITCH-SH-modified electrodes is summarized in Figure 3-11. While the calculated electron transfer rate constants show a moderate increase when the surface density of the DNA switches decreases, there are no significant differences (within the experimental uncertainties as indicated by the distribution of the data points) before and after binding adenosine. It is known that electron transfer rate constants are related to the distance between redox marker and electrode surface, which is influenced by the DNA backbone flexibility and surface density. For comparison, we also plotted the data for MB-COMP-SH- and ssDNA-modified electrodes in Figure 3-11. At high surface density the electron transfer rate constants at MB-SWITCH-SH-, MB-COMP-SH- and ssDNA-modified electrodes are not very different, probably due to rather similar molecular orientations. However, at low surface density, ssDNA has the highest rate constant, and the dsDNA has the smallest rate constant. Given the comparison of k values in the inset of Figure 3-11, we conclude that MB tethered to the DNA switch is not directly reduced on the gold surface even though the DNA switch is more flexible than fully complementary dsDNA.

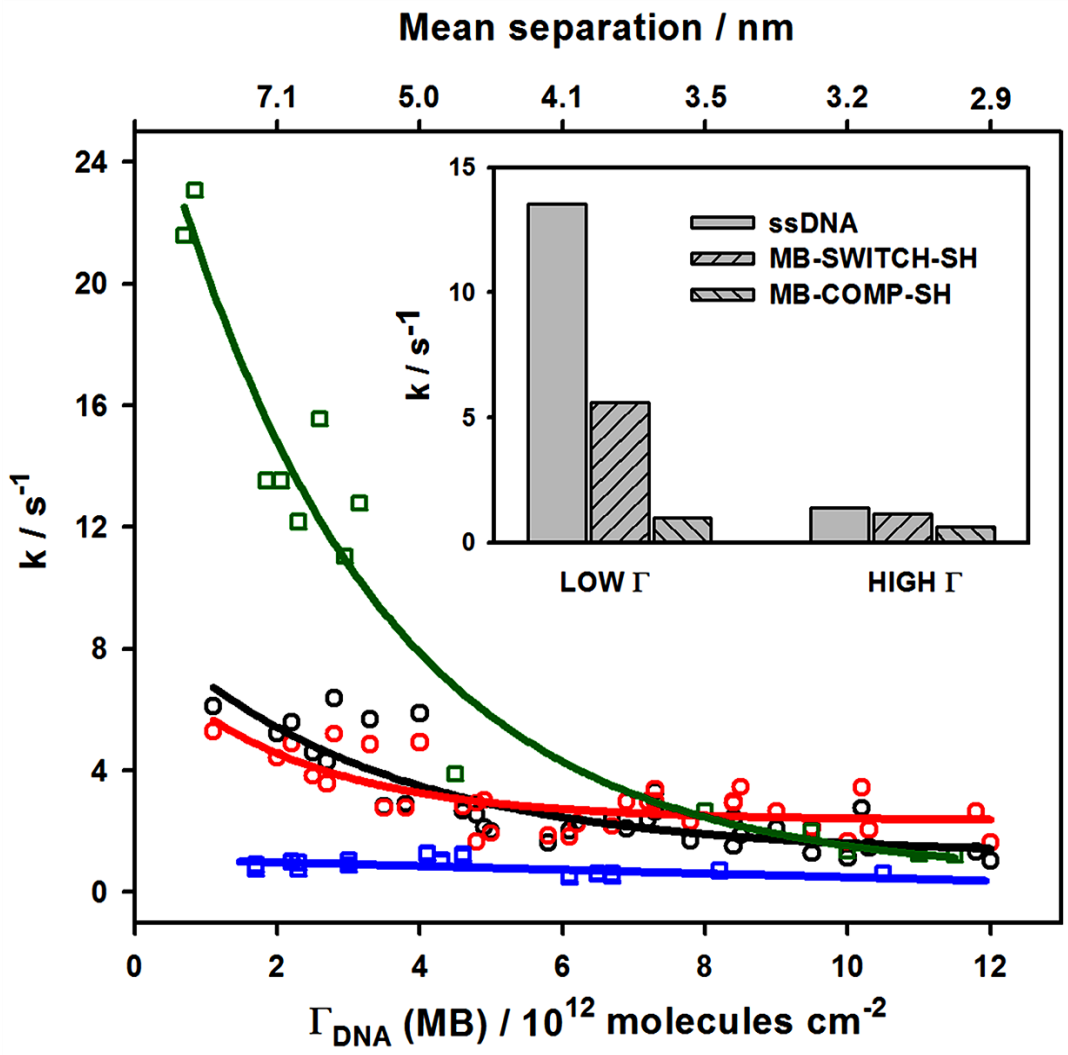

Figure 3-11. Electron transfer rate constant k as function of DNA surface density (Γ_{DNA}) calculated from the integrated charge (peak area) of MB reduction at MB-SWITCH-SH- [before (black line) and after (red line) adding 1.0 mM adenosine], MB-COMP-SH- (blue line), and ssDNA- (green line)modified gold electrodes, respectively. The surface densities of ssDNA shown here have been divided by two to allow direct comparison with the other two systems. The inset shows a comparison of k values at high and low surface densities, respectively.

3.2.3. Intermolecular interactions of DNA

Having proved that neither of the above two factors (electroactivity and electron transfer rate) are responsible for the signal switching, we propose here that lateral intermolecular interactions are the main contributing factor. Closely packed DNA monolayers are formed on gold surfaces by irreversible adsorption because of the strong gold-sulfur interactions. When electroactive species (MB) are tethered to surface-bound DNA, the electrochemical response is affected significantly by lateral interactions between O (oxidized species, MB^+) and O, R (reduced species, LB) and R, O and R[99,102]. If a Frumkin isotherm is obeyed which assumes a random distribution of O and R sites in the film and takes into account the interactions between the molecules, the expression for the current (*i*) is:[99]

$$i = \frac{n^2 F^2 A \upsilon \Gamma_T}{RT} \Psi \qquad \text{(Equation 3-4)}$$

with $\Psi = \frac{f(1-f)}{1-2vg\theta_T f(1-f)}$, and $g = a_O + a_R - 2a_{OR}$, $f = \theta_O / \theta_T$, $\theta_T = \theta_O + \theta_R$.

where a_{OR}, a_O, and a_R are the interaction parameters between O, R, O and R, respectively (a_i is positive for an attractive interaction and a_i is negative for a repulsive one), here a_{OR} and a_R are close to zero as LB is not charged. ν is the number of water molecules displaced by one molecule of O or R, θ_O and θ_R are the coverages of O and R, respectively, *n* is the number of electrons transferred, *A* is the electrode area, υ is the scan rate, and Γ_T is the total surface density of electroactive species.

Because $\Gamma_T = \frac{Q}{nFA}$, $i_P = \frac{nF\upsilon Q}{RT}\Psi_P$ when Ψ reaches the maximum for f = 0.5. Therefore, $vg\theta_T$ can be calculated from the above equations to be -2.6 and -1.7 before and after adding adenosine to high-density MB-SWITCH-SH-modified electrodes (Γ_T = 6.0×10^{12} molecules/cm^2), respectively. Because ν and θ_T are positive

parameters, the negative $vg\theta_T$ indicates repulsive intermolecular interactions (which is reasonable considering the positive charge of MB). After binding to adenosine, the repulsive interactions are strongly reduced leading to a narrower and higher peak. The variations of the function Ψ at two values of $vg\theta_T$ were modeled and compared to the experimental data, which is shown in Figure 3-12. When converting the experimental current *i* at scan rate of 300 mV/s to Ψ by using equation 3-4, the capacitive currents were subtracted from the overall current values and only the Faradic currents were considered. To obtain the theoretical Ψ, a series of f values between 0 and 1 were used with the given $vg\theta_T$. It can be seen that the experimental *i-E* curve (the CV curve of MB reduction) matches the theoretical one well. The discrepancy between the two curves in each pair may be because the DNA-modified surfaces are in fact heterogeneous which is different from the assumption. The modelling for other DNA surface densities also showed similar agreement between the experimental and theoretical curves (data not shown). Furthermore, the peak width δ at mid-height is given by:

$$n\delta = \frac{2RT}{F}\left|\ln\frac{1+\beta}{1-\beta} - vg\theta_T\beta\right| \qquad \text{(Equation 3-5)}$$

$$\beta = \frac{\sqrt{2 - vg\theta_T}}{\sqrt{4 - vg\theta_T}} \qquad \text{(Equation 3-6)}$$

The peak widths δ at half-height before and after ligand binding are calculated to be 0.118 and 0.092 V, respectively. The experimentally determined values are 0.115 and 0.090 V, respectively. The consistency between experimental and theoretical results demonstrates that the variation of the reduction peak shape and current are due to reduced repulsive intermolecular interactions.

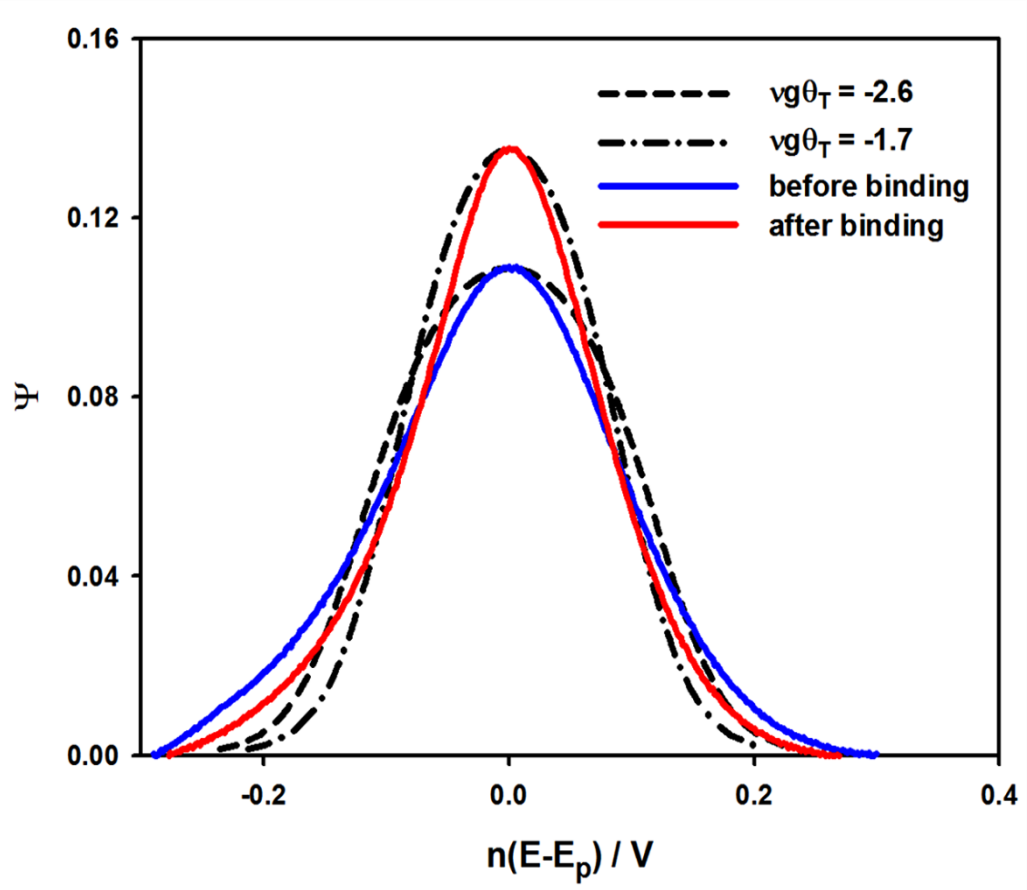

Figure 3-12. Fitted and experimental Ψ values as function of n(E-E_p) for the reduction of MB at a scan rate of 300 mV/s before (blue line) and after (red line) adenosine binding to a high-density MB-SWITCH-SH-modified electrode; the values of $vg\theta_T$ are -2.6 and -1.7 for the two fitted curves. Γ_{DNA} was 1.2×10^{13} molecules/cm^2.

To further evaluate the effect of intermolecular interactions, the interaction parameter $vg\theta_T$ was studied before and after binding adenosine at different surface densities. As shown in Figure 3-13A, at high surface densities (> 4.1×10^{12} molecules/cm^2), $vg\theta_T$ became more positive (i.e., closer to zero) and the repulsive interactions were reduced leading to an increased peak current upon ligand binding; while at low surface densities (< 4.1×10^{12} molecules/cm^2) it became more negative and the repulsive interactions increased leading to a lower peak current. Therefore, the variation of intermolecular interactions supports the bipolar switching behavior observed

in our CV studies. Moreover, no matter surface density is high or low, the DNA switch always changes from close to ssDNA to proximity to dsDNA upon binding adenosine (Figure 3-13C) which is consistent with the formation of a more rigid structure.

The "bipolar" switching properties of our DNA switch have been found to be modulated by lateral intermolecular interactions, presumably due to electrostatic repulsion between MB moieties. Further studies are planned to explore the contribution of interactions between DNA strands themselves. We have prepared diluted MB-SWITCH-SH-modified electrodes by mixing MB-modified strand 1 with unmodified strands. The total concentration of strand 1 remained the same, but the concentration of MB-modified strands was reduced. The interaction parameters $vg\theta_T$ before and after adding adenosine to this "diluted" MB-SWITCH-SH-modified electrode are shown in Figure 3-13B. The surface density calculated from the area of the MB reduction peak was used to examine the concentration of MB-modified DNA constructs in the monolayer. Interestingly, no significant change of $vg\theta_T$ was found when the concentration of MB was lowered in the absence or presence of adenosine except at very low surface density. The total surface density of DNA constructs was obtained by using surface-bound $[Ru(NH_3)_6]^{3+}$, as some of the DNA switches were not labeled. The relationship between $vg\theta_T$ and total DNA surface density for both MB-SWITCH-SH- and diluted MB-SWITCH-SH-modified electrodes is shown in Figure 3-14. As shown in the figure, the total DNA surface density of the diluted MB-SWITCH-SH remained in a rather small range. The $vg\theta_T$ values before and after adding adenosine were consistent with the values obtained for MB-SWITCH-SH. Based on these results, we believe that the intermolecular interactions depend on the total DNA surface density rather than on the concentration of MB molecules. Because MB can couple to the base stack at the ends of DNA strands through intercalation, the interactions between MB molecules in principle follow the same trend as the interactions between DNA strands.

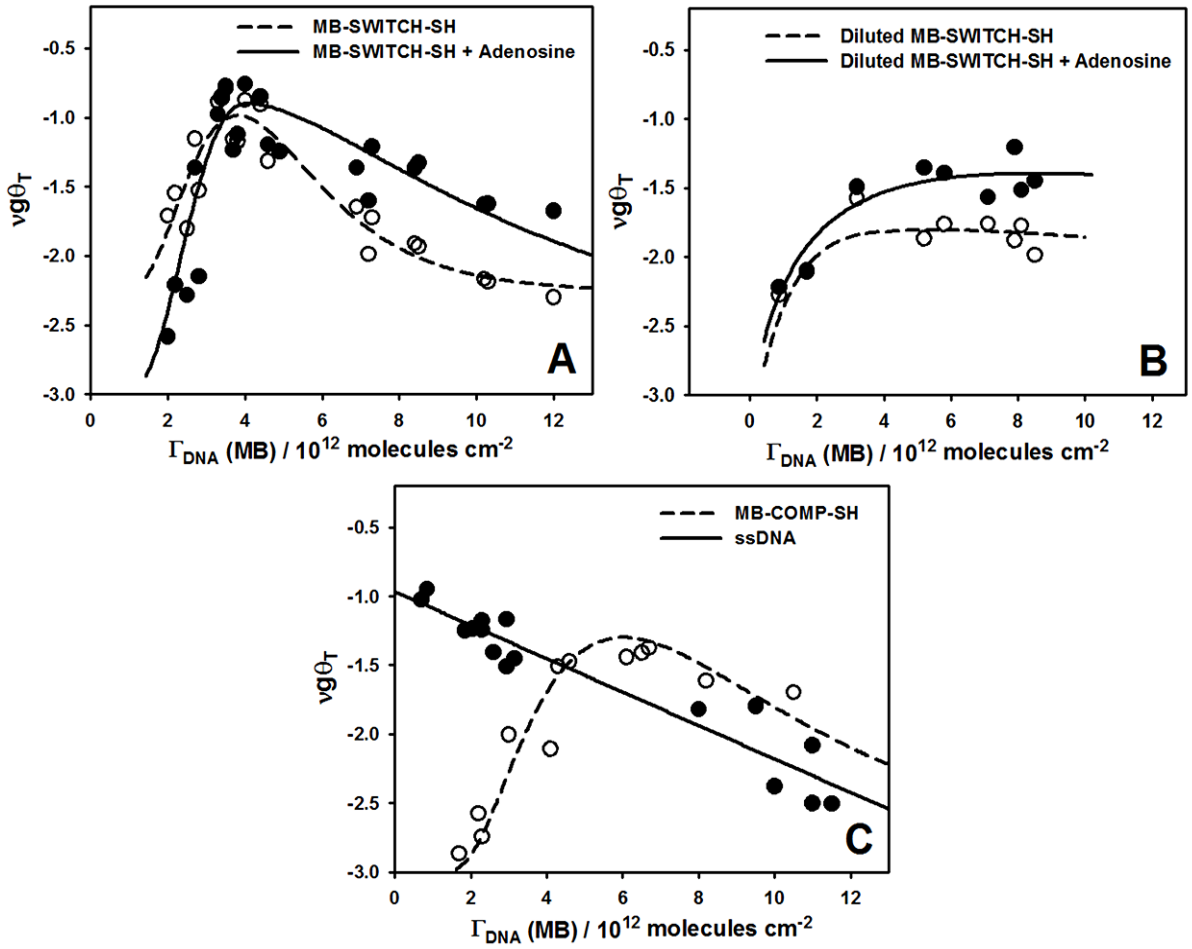

Figure 3-13. Interaction parameter ($vg\theta_T$) before and after adding adenosine as function of DNA surface density (Γ_{DNA}) calculated from the integrated charge (peak area) of MB reduction at (A) MB-SWITCH-SH- and (B) diluted MB-SWITCH-SH-modified electrodes, respectively. (C) Interaction parameter $vg\theta_T$ as function of DNA surface density (Γ_{DNA}) calculated from the integrated charge (peak area) of MB reduction at MB-COMP-SH- (dash line) and ssDNA-(solid line)modified electrodes. The surface densities of ssDNA shown here were divided by two to allow for direct comparison with dsDNA-modified electrodes.

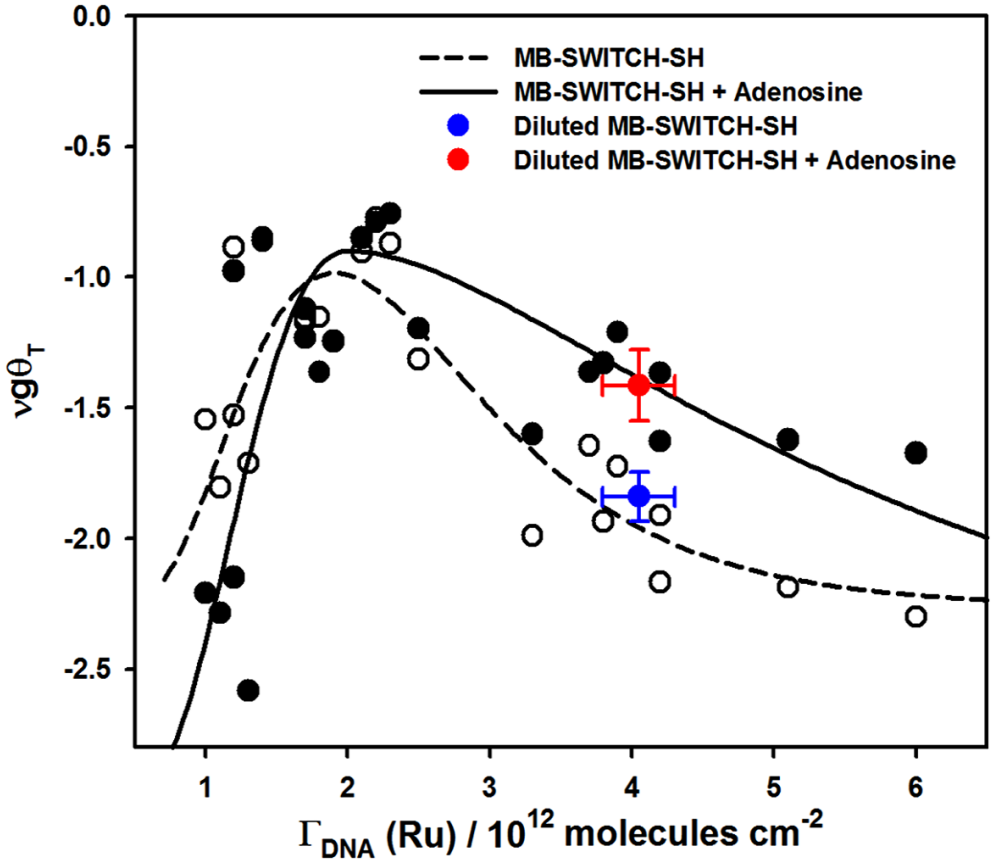

Figure 3-14. Interaction parameter $vg\theta_T$ before (dash line) and after (solid line) binding adenosine as function of DNA surface density (Γ_{DNA}) calculated from the integrated charge (reduction peak area) of surface-bound $[Ru(NH_3)_6]^{3+}$ at MB-SWITCH-SH-modified electrodes. The blue and red dots show the average $vg\theta_T$ values at differently diluted MB-SWITCH-SH-modified electrodes with similar total DNA surface densities. The error bars indicate the range of $vg\theta_T$ and Γ_{DNA}(Ru) for differently diluted MB-SWITCH-SH-modified electrodes.

Based on the hypothesis advanced above, we propose that the redox switching in our DNA construct is dictated by the correlation between molecular orientation and surface density (Scheme 1). At high surface density, the DNA molecules are close to each other inducing strong repulsive interactions. After adding adenosine, the DNA is less flexible leading to a rather uniform distribution of redox centers on the electrode surface, which in turn induces less repulsion and higher peak currents. At low surface

density, the flexible DNA switch structure before binding adenosine permits stacking above the surface resulting in weaker interactions between the MB tethered at the top. Ligand binding makes the DNA construct more rigid and brings the top ends close to each other. Therefore, a stronger repulsive interaction is expected and the peak current decreases. The DNA switch exhibits a unique “bipolar” switching performance with the only variant being surface density: above the value of 4.1×10^{12} molecules/cm^2, it switches on by increasing the peak current; below this value, it switches on by decreasing the peak current. Such a unique electronic switching behavior of DNA constructs in fact mimics the response of a two-way (ON/OFF/ON) electrical switch.

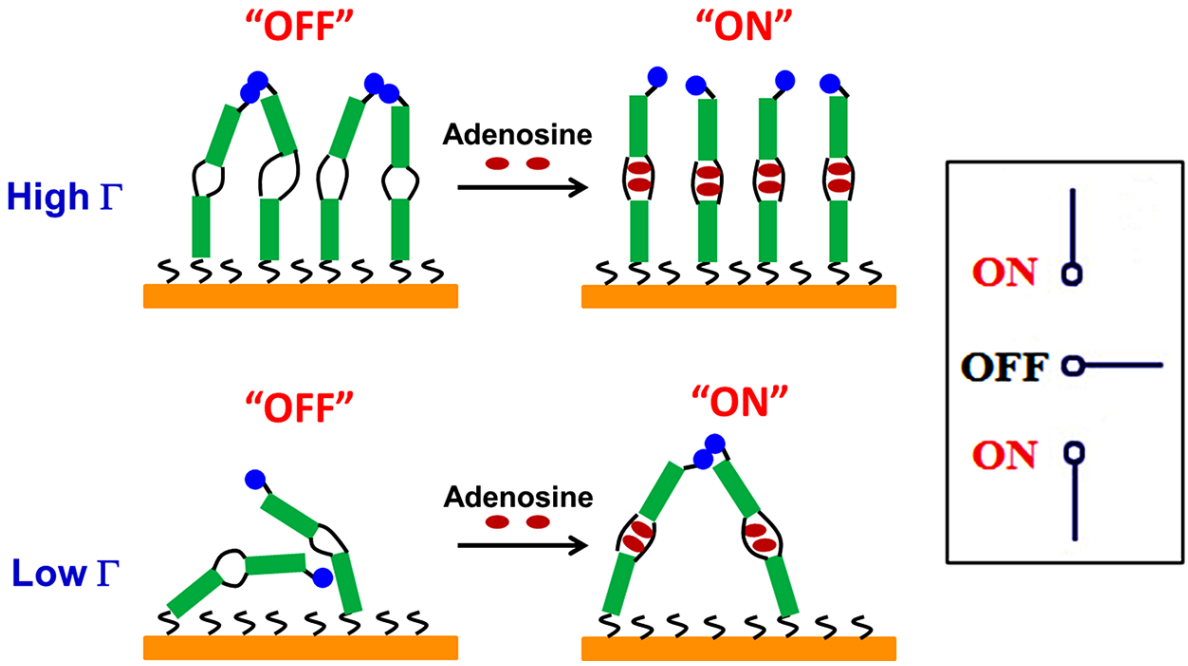

Scheme 1. Schematic representation of the correlation between surface density and molecular orientation in a “bipolar” DNA switch which mimics the behavior of a two-way (ON/OFF/ON) electrical switch.

4. Conclusions and Future Work

4.1. Conclusions

In this work, we have described a unique chip-based “bipolar” DNA switch, for which the two-way switch-on depends on the surface density of the DNA constructs immobilized on the electrode surface. At high surface density, it switches on by increasing the peak current; at low surface density, it switches on by decreasing the peak current. We have not observed any significant variation of either the integrated charge (peak area) or the electron transfer rate constants; only the shape of reduction peak is changed. Electrochemical modeling studies suggest that intermolecular interactions between DNA molecules modulate the signal switching. The study provides further insight into the rather complex electrochemistry of self-assembled DNA monolayers, and also suggests the possibility of designing a new class of biosensors in which analyte binding produces significant changes in intermolecular interactions.

4.2. Future work

To further understand the electron transfer between redox reporter-modified self-assembled DNA monolayers and gold electrode surfaces, many different designs of DNA switches or devices need to be studied. The redox reporter MB can be modified at different positions of the DNA strand. The adenosine aptamer-based switch is a model of a chip-based double-stranded DNA switch. Another double-stranded DNA switch with cocaine aptamer will be studied.

References

(1) Seeman, N. C. *Biochemistry* **2003**, *42*, 7259-7269.

(2) Park, S. H.; Barish, R.; Li, H. Y.; Reif, J. H.; Finkelstein, G.; Yan, H.; LaBean, T. H. *Nano Lett.* **2005**, *5*, 693-696.

(3) Seeman, N. C. *Trends Biochem. Sci.* **2005**, *30*, 119-125.

(4) Bath, J.; Turberfield, A. J. *Nat. Nanotech.* **2007**, *2*, 275-284.

(5) Seeman, N. C. *Annu. Rev. Biochem.* **2010**, *79*, 65-87.

(6) Mao, C. D.; Sun, W. Q.; Shen, Z. Y.; Seeman, N. C. *Nature* **1999**, *397*, 144-146.

(7) Yang, Y.; Liu, G.; Liu, H.; Li, D.; Fan, C.; Liu, D. *Nano Lett.* **2010**, *10*, 1393-1397.

(8) Chen, Y.; Wang M.; Mao, C. D. *Angew. Chem. Int. Ed.* **2004**, *43*, 3554-3557.

(9) Niemeyer, C. M.; Adler, M.; Lenhert, S.; Gao, S.; Fuchs, H.; Chi, L. F. *ChemBioChem* **2001**, *2*, 260-264.

(10) Shin, J. S.; Pierce, N. A. *J. Am. Chem. Soc.* **2004**, *126*, 10834-10835.

(11) Yin, P.; Yan, H.; Daniell, X. G.; Turberfield, A. J.; Reif, J. H. *Angew. Chem. Int. Ed.* **2004**, *43*, 4906-4911.

(12) Ellington, A. D.; Szostak, J. W. *Nature* **1990**, *346*, 818-822.

(13) Tuerk, C.; Gold, L. *Science* **1990**, *249*, 505-510.

(14) Bock, L. C.; Griffin, L. C.; Latham, J. A.; Vermaas, E. H.; Toole, J. J. *Nature* **1992**, *355*, 564-566.

(15) Ekland, E. H.; Szostak, J. W.; Bartel, D. P. *Science* **1995**, *269*, 364-370.

(16) Zhang, B. L.; Cech, T. R. *Nature* **1997**, *390*, 96-100.

(17) Simmel, F. C.; Dittmer, W. U. *Small* **2005**, *1*, 284-299.

(18) Padmanabhan, K.; Padmanabhan, K. P.; Ferrara, J. D.; Sadler, J. E.; Tulinsky, A. *J. Biol. Chem.* **1993**, *268*, 17651-17654.

(19) Stojanovic, M. N.; de Prada, P.; Landry, D. W. *J. Am. Chem. Soc.* **2000**, *122*, 11547-11548.

(20) Hermann, T.; Patel, D. J. *Science* **2000**, *287*, 820-825.

(21) Sefah, K.; Shangguan, D.; Xiong, X.; O'Donoghue M. B.; Tan, W. *Nat. Protoc.* **2010**, *5*, 1169-1185.

(22) Ellington, A. D.; Szostak, J. W. *Nature* **1990**, *346*, 818-822.

(23) Tuerk, C.; Gold, L. *Science* **1990**, *249*, 505-510.

(24) Tombelli, S.; Minunni, M.; Mascini, M. *Biomol. Eng.* **2007**, *24*, 191-200.

(25) Homann, M.; Goringer, H. U. *Nucleic Acids Res.* **1999**, *27*, 2006-2014.

(26) Osborne, S. E.; Ellington, A. D. *Chem. Rev.* **1997**, *97*, 349-370.

(27) Hamula, C. L. A.; Guthrie, J. W.; Zhang, H. Q.; Li, X. F.; Le, X. C. *Trends Anal. Chem.* **2006**, *25*, 681-691.

(28) Cass, A. E. G.; Zhang, Y. *Faraday Discuss.* **2011**, *149*, 49-61.

(29) O'Sullivan, C. K. *Anal. Bioanal. Chem.* **2002**, *372*, 44-48.

(30) Herne, T. M.; Tarlov, M. J. *J. Am. Chem. Soc.* **1997**, *119*, 8916-8920.

(31) Steel, A. B.; Herne, T. M.; Tarlov, M. J. *Anal. Chem.* **1998**, *70*, 4670-4677.

(32) Gorodetsky, A. A.; Buzzeo, M. C.; Barton, J. K. *Bioconjugate Chem.* **2008**, *19*, 2285-2296.

(33) Mayer, G. *Angew. Chem. Int. Ed.* **2009**, *48*, 2672-2689

(34) Lin, J. C.; Thirumalai, D. *J. Am. Chem. Soc.* **2008**, *130*, 14080-14081.

(35) Ellington, A. D.; Szostak, J. W. *Nature* **1992**, *355*, 850-852.

(36) Neves, M. A. D.; Reinstein, O.; Saad, M.; Johnson, P. E. *Biophys. Chem.* **2010**, *153*, 9-16.

(37) Tombelli, S.; Minunni, M.; Mascini, M. *Biomol. Eng.* **2007**, *24*, 191-200.

(38) Homann, M.; Goringer, H. U. *Nucleic Acids Res.* **1999**, *27*, 2006-2014.

(39) Silverman, S. K. *Acc. Chem. Res.* **2009**, *42*, 1521-1531.

(40) Silverman, S. K. *Nucleic Acids Res.* **2005**, *33*, 6151-6163.

(41) Liu J.; Lu, Y. *J. Am. Chem. Soc.* **2007**, *129*, 9838-9839.

(42) Silverman, S. K. *Org. Biomol. Chem.* **2004**, *2*, 2701-2705.

(43) Zhou, M.; Kuralay, F.; Windmiller, J. R.; Wang, J. *Chem. Commun.* **2012**, *48*, 3815-3817.

(44) Vannela, R.; Adriaens, P. *Environ. Sci. Technol.* **2006**, *36*, 375-381.

(45) Alberti, P.; Bourdoncle, A.; Saca, B.; Lacroix, L.; Mergny, J. L. Org. *Biomol. Chem.* **2006**, *4*, 3383-3391.

(46) Bock, L. C.; Griffin, L. C.; Latham, J. A.; Vermaas, E. H.; Toole, J. J. *Nature* **1992**, *355*, 564-566.

(47) Kelly, J. A.; Feigon, J.; Yeates, T. O. *J. Mol. Biol.* **1996**, *256*, 417-422.

(48) Gehring, K.; Leroy, J. L.; Gueron, M. *Nature* **1993**, *363*, 561-565.

(49) Liu, D.; Balasubramanian, S. *Angew. Chem. Int. Ed.* **2003**, *42*, 5734-5736.

(50) Drummond, T. G.; Hill, M. G.; Barton, J. K. *Nature Biotech.* **2003**, *21*, 1192-1199.

(51) March, G.; Noel, V.; Piro, B.; Reisberg, S.; Pham, M. *J. Am. Chem. Soc.* **2008**, *130*, 15752-15753.

(52) Zhang, Y.; Wang, Y.; Wang, H.; Jiang, J.; Shen, G.; Yu, R.; Li, J. *Anal. Chem.* **2009**, *81*, 1982-1987.

(53) Zhong, X.; Bai, H.; Xu, J.; Chen, H.; Zhu, Y. *Adv. Funct. Mater.* **2010**, *20*, 992-999.

(54) Radi, A. E.; Sánchez, J. L. A.; Baldrich, E.; O'Sullivan, C. K. *Anal. Chem.* **2005**, *77*, 6320-6323.

(55) Lai, R. Y.; Seferos, D. S.; Heeger, A. J.; Bazan, G. C.; Plaxco, K. W. *Langmuir* **2006**, *22*, 10796-10800.

(56) White, R. J.; Phares, N.; Lubin, A. A.; Xiao, Y.; Plaxco, K. W. *Langmuir* **2008**, *24*, 10513-10518.

(57) Ihara, T.; Maruo, Y.; Takenaka, S.; Takagi, M. *Nucleic Acids Res.* **1996**, *24*, 4273-4280.

(58) Pheeney, C. G.; Barton, J. K. *Langmuir* **2012**, *28*, 7063-7070.

(59) Kelley, S. O.; Jackson, N. M.; Hill, M. G.; Barton, J. K. *Angew. Chem. Int. Ed.* **1999**, *38*, 941-945.

(60) Kelley, S. O.; Boon, E. M.; Barton, J. K.; Jackson, N. M.; Hill, M. G. *Nucleic Acids Res.* **1999**, *27*, 4830-4837.

(61) Kelley, S. O.; Barton, J. K. *Bioconjugate Chem.* **1997**, *8*, 31-37.

(62) Rodriguez, M. C.; Kawde, A. N.; Wang, J. *Chem. Commun.* **2005**, *34*, 4267-4269.

(63) Yu, H.-Z.; Luo, C.-Y.; Sankar, C. G.; Sen, D. *Anal. Chem.* **2003**, *75*, 3902-3907.

(64) Ge, B.; Huang, Y.-C.; Sen, D.; Yu, H.-Z. *J. Electroanal. Chem.* **2007**, *602*, 156-162.

(65) Cheng, A. K. H.; Ge, B.; Yu, H.-Z. *Anal. Chem.* **2007**, *79*, 5158-5164.

(66) Huizenga, D. E.; Szostak, J. W. *Biochemistry* **1995**, *34*, 656-665.

(67) Lin, C. H.; Patel, D. J. *Chem. Biol.* **1997**, *4*, 817-832.

(68) Cheng, A. K. H.; Sen, D.; Yu, H.-Z. *Bioelectrochemistry* **2009**, *77*, 1-12.

(69) Zuo, X.; Song, S.; Zhang, J.; Pan, D.; Wang, L.; Fan, C. *J. Am. Chem. Soc.* **2007**, *129*, 1042-1043.

(70) Liu, Z.; Yuan, R.; Chai, Y.; Zhuo, Y.; Hong, C.; Yang, X.; Su, H.; Qian, X. *Electrochim. Acta* **2009**, *54*, 6207-6211.

(71) Shen, L.; Chen, Z.; Li, Y.; Jing, P.; Xie, S.; He, S.; He, P.; Shao, Y. *Chem. Commun.* **2007**, *21*, 2169-2171.

(72) Chakraborty, B.; Jiang, Z.; Li, Y.; Yu, H.-Z. *J. Electroanal. Chem.* **2009**, *635*, 75-82.

(73) Zayats, M.; Huang, Y.; Gill, R.; Ma, C.; Willner, I. *J. Am. Chem. Soc.* **2006**, *128*, 13666-13667.

(74) Wang, J.; Wang, F.; Dong, S. *J. Electroanal. Chem.* **2009**, *626*, 1-5.

(75) Tasset, D. M.; Kubik, M. F.; Steiner, W. *J. Mol. Bio.* **1997**, *272*, 688-698.

(76) Wang, K. Y.; McCurdy, S.; Shea, R. G.; Swaminathan, S.; Bolton, P. H. *Biochemistry* **1993**, *32*, 1899-1904.

(77) Macaya, R. F.; Waldron, J. A.; Beutel, B. A.; Gao, H. T.; Joesten, M. E.; Yang, M. H.; Patel, R.; Bertelsen, A. H.; Cook, A. F. *Biochemistry* **1995**, *34*, 4478-4492.

(78) Lu, Y.; Li, X.; Zhang, L.; Yu, P.; Su, L.; Mao, L. *Anal. Chem.* **2008**, *80*, 1883-1890.

(79) Lu, Y.; Zhu, N.; Yu, P.; Mao, L. *Analyst* **2008**, *133*, 1256-1260.

(80) Xiao, Y.; Lubin, A. A.; Heeger, A. J.; Plaxco, K. W. *Angew. Chem. Int. Ed.* **2005**, *44*, 5456-5459.

(81) Baker, B. R.; Lai, R. Y.; Wood, M. S.; Doctor, E. H.; Heeger, A. J.; Plaxco, K. W. *J. Am. Chem. Soc.* **2006**, *128*, 3138-3139.

(82) Radi, A. E.; Acero Sánchez, J. L.; Baldrich, E.; O'Sullivan, C. K. *J. Am. Chem. Soc.* **2005**, *128*, 117-124.

(83) Zhang, X.-B.; Kong, R.-M.; Lu, Y. *Annu. Rev. Anal. Chem.* **2011**, *4*, 105-128.

(84) Xiao, Y.; Rowe, A. A.; Plaxco, K. W. *J. Am. Chem. Soc.* **2007**, *129*, 262-263.

(85) Liang, J.; Chen, Z.; Guo, L.; Li, L. *Chem. Commun.* **2011**, *47*, 5476-5478.

(86) Gao, X.; Huang, H.; Niu, S.; Ye, H.; Lin, Z.; Qiu, B.; Chen, G. *Anal. Methods* **2012**, *4*, 947-952.

(87) Shen, L.; Chen, Z.; Li, Y.; He, S.; Xie, S.; Xu, X.; Liang, Z.; Meng, X.; Li, Q.; Zhu, Z.; Li, M.; Le, X. C.; Shao, Y. *Anal. Chem.* **2008**, *80*, 6323-6328.

(88) Lin, Z.; Chen, Y.; Li, X.; Fang, W. *Analyst* **2011**, *136*, 2367-2372.

(89) Shin, S. R.; Lee, C. K.; Lee, S. H.; Kim, S. I.; Spinks, G. M.; Wallace, G. G.; So, I.; Jeong, J.-H.; Kang, T. M.; Kim, S. *Chem. Commun.* **2009**, *10*, 1240-1242.

(90) Huang, Y. C.; Sen, D. *J. Am. Chem. Soc.* **2010**, *132*, 2663-2671.

(91) Ge, B.; Huang, Y. C.; Sen, D.; Yu, H.-Z. *Angew. Chem. Int. Ed.* **2010**, *49*, 9965-9967.

(92) Anne, A.; Demaille, C. *J. Am. Chem. Soc.* **2006**, *128*, 542-557.

(93) Anne, A.; Demaille, C. *J. Am. Chem. Soc.* **2008**, *130*, 9812-9823.

(94) Huang, Y. C.; Ge, B.; Sen, D.; Yu, H.-Z. *J. Am. Chem. Soc.* **2008**, *130*, 8023-8029.

(95) Fahlman, R. P.; Sen, D. *J. Am. Chem. Soc.* **2002**, *124*, 4610-4616.

(96) Boon, E. M.; Jackson, N. M.; Wightman, M. D.; Kelley, S. O.; Hill, M. G.; Barton, J. K. *J. Phys. Chem. B* **2003**, *107*, 11805-11812.

(97) Lu, N.; Pei, H.; Ge, Z.; Simmons, C. R.; Yan, H.; Fan, C. *J. Am. Chem. Soc.* **2012**, *134*, 13148-13151.

(98) Abi, A.; Ferapontova, E. E. *J. Am. Chem. Soc.* **2012**, *134*, 14499-14507.

(99) Laviron, E. *J. Electroanal. Chem.* **1974**, *52*, 395-402.

(100) Long, Y. T.; Li, C. Z.; Sutherland, T. C.; Chahma, M.; Lee, J. S.; Kraatz, H. B. *J. Am. Chem. Soc.* **2003**, *125*, 8724-8725.

(101) Ricci, F.; Lai, R. Y.; Heeger, A. J.; Plaxco, K. W.; Sumner, J. J. *Langmuir* **2007**, *23*, 6827-6834.

(102) Bard, A. J.; Faulkner, L. R. *Electrochemical Methods: Fundamentals and Applications*, 2nd ed.; John Wiley & Sons: New York, **2001**.

(103) Peng, W. F.; Rusling, J. F. *J. Phys. Chem.* **1995**, *99*, 16436-16441.

(104) Dale, N.; Pearson, T.; Frenguelli, B. G. *J. Physiol.* **2000**, *526*, 143-155.

(105) Dale, N.; Gilday, D. *Nature* **1996**, *383*, 259-263.

(106) Porkka-Heiskanen, T. *Ann. Med.* **1999**, *31*, 125-129.

(107) Wu, Z. S.; Guo, M. M.; Zhang, S. B.; Chen, C. R.; Jiang, J. H.; Shen, G. L.; Yu, R. Q. *Anal. Chem.* **2007**, *79*, 2933-2939.

(108) Du, Y.; Chen, C. G.; Zhou, M.; Dong, S. J.; Wang, E. K. *Anal. Chem.* **2011**, *83*, 1523-1529.

(109) Laviron, E. *J. Electroanal. Chem.* **1979**, *101*, 19-28.

Appendices

Appendix A.

Intrinsic-ligand DNA switch for cocaine

Hypothesis

Besides “integrated-ligand” and “coupled-ligand” DNA switches, we also designed another kind of DNA switch which are “intrinsic-ligand” DNA switches. These switches contain a three-way junction formed by two DNA strands similar to “coupled-ligand” DNA switches. However, the whole DNA construct is aptamer and the ligand binding domain is at the junction which are the differences between “intrinsic-ligand” and “coupled-ligand” DNA switches. When immobilizing the redox reporter modified “intrinsic-ligand” DNA switches onto gold electrode surfaces, the electron transfer through DNA can be studied before and after ligand binding.

The cocaine aptamer has become a well-developed template for a wide range of different biosensor technologies including optical, electrochemical and spectroscopic ones[1-4]. This aptamer is composed of three stems that meet at three-way junction. Baker et al. fabricated an electrochemical sensor for the detection of cocaine based on single-stranded cocaine aptamer[5]. The folding of aptamer brought the redox reporter close to the electrode surface. The redox-to-surface distance change resulted in the signal switching. Du et al. divided the aptamer into two separate strands[6]. The hybridization of two strands and the cocaine binding lead to a decreased signal in a layer-by-layer (LBL) self-assembled multilayer with ferrocene-appended poly(ethyleneimine) (Fc-PEI) on an indium tin oxide (ITO) array electrode.

In this work, we also used a two-stranded cocaine aptamer to construct the “intrinsic-ligand” DNA switches. Instead of introducing the second strand together with cocaine, we immobilized both strands on gold electrode surfaces. The two strands of cocaine aptamer form a three-way junction and methylene blue (MB) is modified at the end of one strand as redox reporter for the electrochemical monitoring (Figure A-1). The electron transfer is poor because of the lack of base stacking in the junction before cocaine binding. However, when cocaine binds to the junction, the structural switching may result in enhanced electron transfer through the pathway. The electrical current is expected to increase with the concentration of cocaine for the detection.

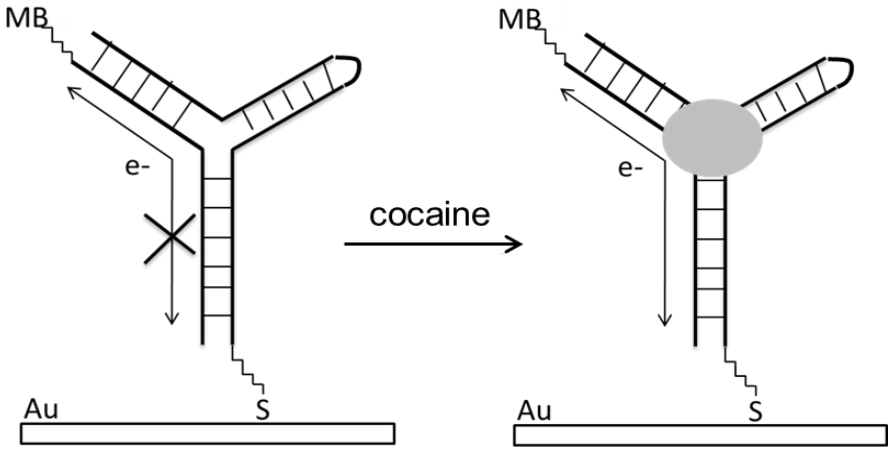

Figure A-1. The hypothetical mechanism of “intrinsic-ligand” DNA switches for cocaine

Experimental Section

The experimental section of this work is the same as Chapter 2 except the DNA sequences and standard buffer used are different. The standard buffer here is 20 mM Tris, 100 mM NaCl, 5 mM $MgCl_2$ at pH 7.4. Strands 1 and 2 were used to construct the switch and strand 1 and 3 were used to prepare the fully complementary duplex as negative control. The sequences of the three strands are as follows:

Strand 1 (thiol modified DNA): 5'-[HO-$(CH_2)_6$-S-S-$(CH_2)_6$-O]-GGC GTC AAG GAA AAT CCT TCA ACT TC-3'

Strand 2: (MB modified DNA): 5'-[MB-(NH-C_6-acrylamido-T)]-GAA GTG GGA CGC C-3'

Strand 3 (thiol modified DNA): 5'-[HO-$(CH_2)_6$-S-S-$(CH_2)_6$-O]-GGC GTC CCA CTT C-3'

Results and Discussions

The "intrinsic-ligand" DNA switch contains a three-way junction, the cocaine aptamer sequence (Figure A-2A) formed by hybridize strand 1 and 2. Methylene blue (MB) was covalently tethered to the 5'-terminus of strand 2 as the redox marker. The 5'-end of strand 1 was modified with a thiol group, enabling the formation of robust DNA self-assembled monolayers on a gold electrode via sulfur-gold linkages. A complete Watson-Crick base-paired double helix formed by strand 2 and its fully complementary strand 3 were used as a control after immobilization on gold surface (Figure A-2B).

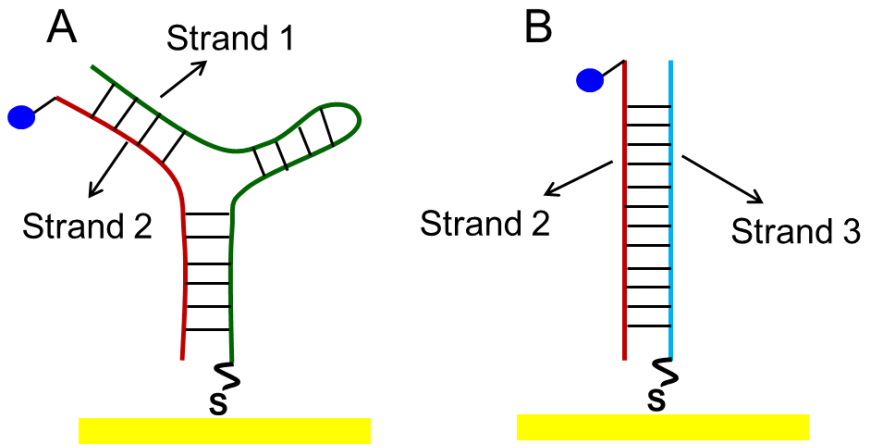

Figure A-2. The schematic design of (A) "intrinsic-ligand" DNA switches for cocaine and (B) negative control

Cyclic voltammetry (CV) and square wave voltammetry (SWV) were used to monitor the changes in reduction current of MB upon binding cocaine for the DNA switch at different surface densities. At low surface density ($1.5\sim2.5\times10^{12}$ molecules/cm^2), the MB reduction peak in CV is weak and SWV showed much better signals (Figure A-3). After the signal became stable in blank standard buffer, different concentration of cocaine was added into the buffer. There was only slight increase in the MB reduction peak upon cocaine binding. This may due to two reasons. First, compared to "integrated-ligand" switches, the "intrinsic-ligand" switches have more complicated DNA structures as well as the electron transfer pattern through DNA. MB is modified on the different DNA strand from thiol, so electron transfer efficiency is not as good as intra-strand. Moreover, the conformational changes at three-way junction before and after cocaine

binding were studied by NMR[7] and it was shown that the structural changes were not significant (Figure A-4).

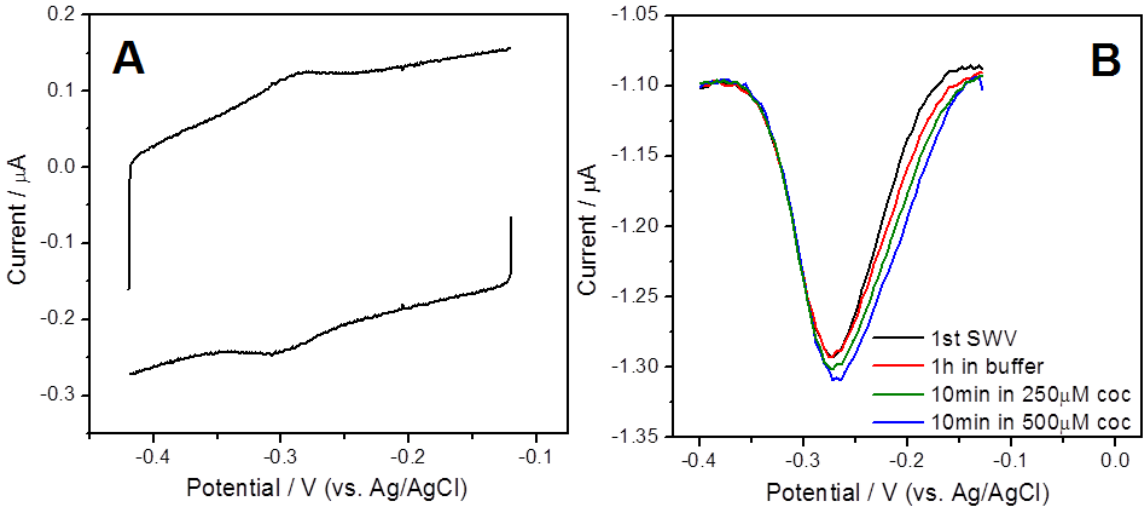

Figure A-3. (A) CV of "intrinsic-ligand" DNA switch and (B) SWV before and after cocaine binding at low surface density

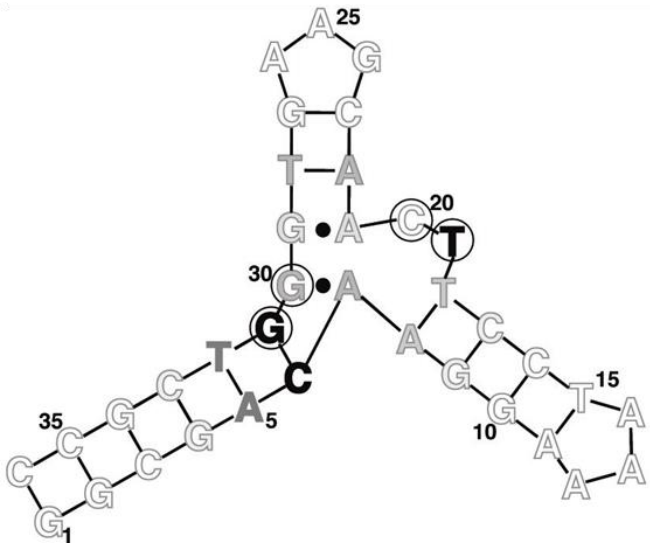

Figure A-4. Chemical shift perturbations mapped onto the secondary structure of the cocaine aptamer. The residues that move most are shown in shades of gray, with the residues that move the most shown in black and those that do not shift shown inwhite.T19,which is only observable in the cocaine bound conformation, is also shown in black. Nucleotides that are circled show intermolecular NOEs to the aromatic ring on cocaine. Reprinted with permission from (7). Copyright (2010) American Chemical Society.

The changes in reduction current of MB upon binding cocaine for the DNA switch at high surface densities (4~5×10^{12} molecules/cm^2) were also investigated by CV and SWV. The MB reduction peak in CV is stronger than that at low surface densities (Figure A-5A). However, the electrochemical signal was not stable with time (Figure A-5B). Both reduction and oxidation peak currents of MB decreased significantly after one hour incubation in blank buffer. This indicates that the DNA constructs of the switch may be unstable on the gold surface, or the hybridization of the two strands may be unfavorable.

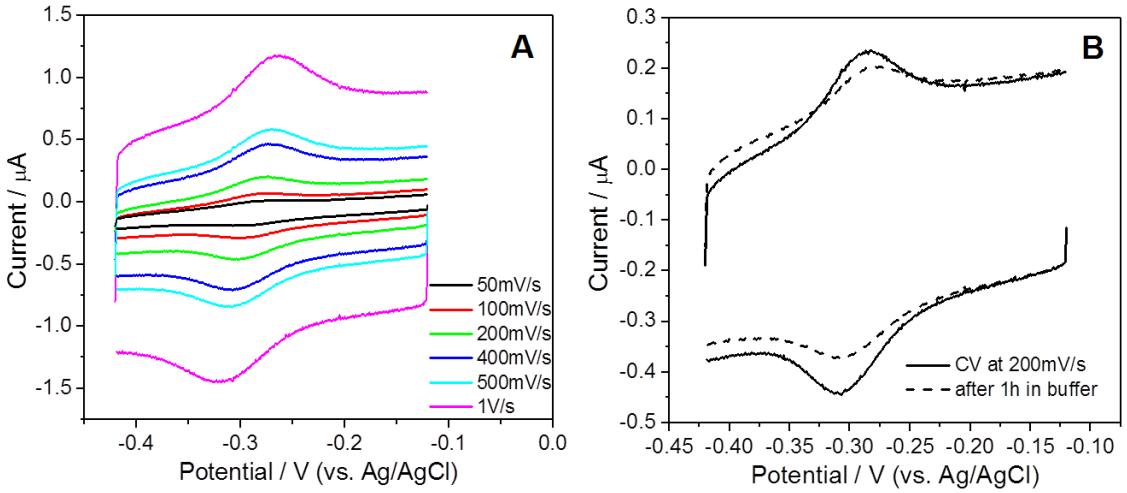

Figure A-5. (A) CV of "intrinsic-ligand" DNA switch at different scan rates and (B) CV comparison after 1h incubation in buffer at high surface density

To make sure if the two strands comprised of the DNA switch and the control system are hybridized to form the DNA constructs we expected, gel electrophoresis of the three single strands (strand 1, 2, 3), the products of hybridization of strands 1 and 2 or strands 2 and 3 in the absence and presence of cocaine, was conducted and shown in Figure A-6.

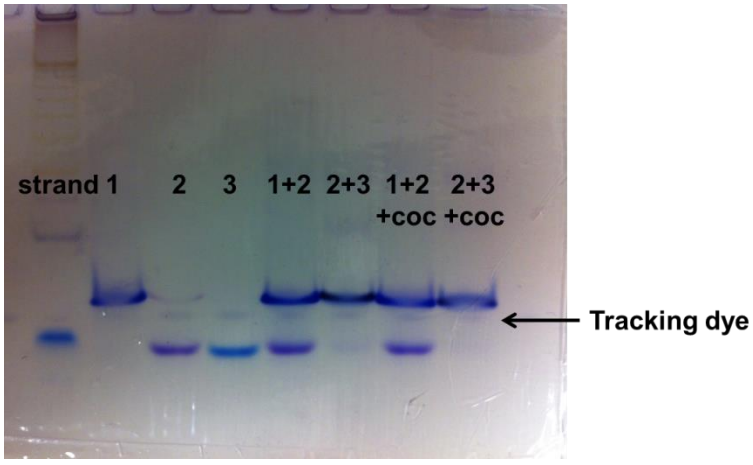

Figure A-6. Gel electrophoresis of single strands (strands 1, 2, 3), and the products of hybridization of strands 1 and 2 or strands 2 and 3 in the absence and presence of cocaine.

It was observed that the fully complementary strands 2 and 3 were hybridized to form the duplex even in the absence of cocaine. However, strands 1 and 2 didn't show hybridization no matter in the absence and presence of cocaine. This indicates that the formation of DNA constructs by strands 1 and 2 is not stable which may be the reason for the decreasing electrochemical signal with time.

Conclusions and Future Work

The "intrinsic-ligand" DNA switches are consisted of the cocaine aptamer which contains a three-way junction. Because of the complexity of its design, the stability of the DNA constructs varies for different sequences, and the electron transfer through DNA can have three different pathways. Besides, the conformational changes at the junction upon cocaine binding are not significant based on NMR analysis. Due to the good sensitivity of electrochemical method, however, the design of the DNA switch can be still optimized to achieve a significant signal switching before and after cocaine binding.

References

(1) Stojanovic, M. N.; Prada, P. de; Landry, D. W. *J. Am. Chem. Soc.* **2000**, *122*, 11547-11548.

(2) Stojanovic, M. N.; Prada, P. de; Landry, D. W. *J. Am. Chem. Soc.* **2001**, *123*, 4928-4931.

(3) Stojanovic, M. N.; Landry, D. W. *J. Am. Chem. Soc.* **2002**, *124*, 9678-9679.

(4) He, J. E.; Wu, Z. H.; Zhou, H.; Wang, H.-Q.; Jiang, J.-H.; Shen, G.-L.; Yu, Q. R. *Anal. Chem.* **2010**, *82*, 1135-1358.

(5) Baker, B. R.; Lai, R. Y.; Wood, M. S.; Doctor, E. H.; Heeger, A. J.; Plaxco, K. W. *J. Am. Chem. Soc.* **2006**, *128*, 3138-3139.

(6) Du, Y.; Chen, C.; Yin, J.; Li, B.; Zhou, M.; Dong, S.; Wang, E. *Anal. Chem.* **2010**, *82*, 1556-1563.

(7) Neves, M. A. D.; Reinstein, O.; Johnson, P. E. *Biochemistry* **2010**, *49*, 8478-8487.